DOCTOR OF PHILOSOPHY

Impact of sea level rise, land reclamation and tidal power plants on regional tidal dynamics

Pelling, Holly

Award date:
2014

Awarding institution:
Bangor University

[Link to publication](#)

Impact of sea level rise, land reclamation and tidal power plants on regional tidal dynamics

Holly E. Pelling

Supervisor: Mattias Green

Co-supervisor: Tom Rippeth

School of Ocean Science

Bangor University

Menai Bridge, Wales

Abstract

The response of regional tidal dynamics to sea level rise (SLR), tidal power plants (TPPs), land reclamation and a combination of the above was investigated using two tidal models. The impact of SLR was investigated on, and tidal models validated for, the European Shelf, the Bay of Fundy and the Bohai Sea. The tidal response varied greatly between regions; however the method in which SLR was implemented within the tidal models also caused significant variation in the response. When sea level was increased but no land was allowed to flood (i.e. the coastline did not move) the change in tidal by processes that involved the increased water depth (such as tidal resonance). However, when land was allowed to flood the response was governed by the change in the spatial distribution of tidal energy dissipation.

The maximum extractable tidal energy and the impact of the extraction of this energy in the Minas Passage were investigated on the tidal regime of the Bay of Fundy. It was found that the impacts were significant and wide spread. Furthermore, it was demonstrated that SLR could increase the maximum extractable tidal energy. The tides of the Bay of Fundy are close to resonance and SLR with no flooding caused the system to move closer to resonance. However when flooding was enabled the system did not move towards resonance, suggesting the change in tidal dissipation dampened the response.

The Bohai Sea has undergone rapid and extensive natural and anthropogenic land reclamation. Tidal gauge observations show that the tidal regime has responded significantly to these changes. We have been able to reproduce these changes using a tidal model, furthermore, future simulations show that the tides of the Bohai Sea may have become more sensitive to impacts of SLR.

It was found that the regional tides investigated were particularly sensitive to changes in the spatial distribution of ideal energy dissipation. As demonstrated by the investigation of practical scenarios.

Key words: Tidal modelling, Tidal power plants, Sea level rise, Land reclamation, Tidal dynamics

Acknowledgements

Preface

This thesis consists of three parts. Part I discusses background theory relevant to the thesis, Part II is a summary of the thesis and fits the papers of Part III into current literature. The following appended papers (Part III) are referred to by their Roman numerals:

Paper I: H.E. Pelling, J.A.M Green and S.L. Ward, 2013: Sea level rise and tides: to flood or not to flood. *Ocean Modeling*, (63), 21–29.

Paper II: H.E. Pelling and J.A.M. Green, 2013: Sea level rise, tidal power plants and resonance in the Gulf of Maine. *Journal of Geophysical Research*,(118), 1–11.

Paper III: H.E. Pelling, K. Uehara, and J.A.M. Green, 2013: The impact of rapid coastline changes and sea level rise on the tides in the Bohai Sea, China. *Journal of Geophysical Research*,(118), 3462–3472.

Paper IV: H.E Pelling and J.A.M. Green, 2013: Impact of flood defences and sea-level rise on the European Shelf tidal regime. *Continental Shelf Research*. Submitted.

An additional paper was prepared during the PhD. It does not form part of the thesis but is mentioned in order to show how the time was used.

Paper V: S.L Ward, J.A.M. Green and H.E Pelling, 2012: Tides, sea-level rise and tidal power extraction on the European shelf. *Ocean Dynamics*,(62), 1153–1167.

Publication work allocation

The main part of Paper I was written by Pelling who also made the model runs and data analysis. Green co-wrote and assisted in the data analysis.

Paper II is based on an idea by Green, who also contributed to the writing. Pelling wrote the paper, and did the model runs, Tidal power plant implementation and data analysis.

Paper III is based on an idea by Uehara and Pelling. Uehara provided the bathymetries, Pelling did the model runs and data analysis and wrote the paper. Green provided writing assistance.

Paper IV was written by Pelling and based on an idea developed by Pelling. The runs and data analysis was conducted by Pelling. Green assisted with the writing and dissipation calculations.

Contents

Part I

Part I: Background Theory

'Essentially, all models are wrong, but some are useful'

E.P. Box (1987)

1 Introduction

In 2003 almost half of the world's population lived in close proximity to the coast, with the expectation that this figure will increase into the next century (Creel, 2003, see also Fig 1.1). Shelf seas are used for a wide variety of human activities, with significant social and economic benefits. Almost 99% of the worlds fish stocks are caught on shelf seas (UNEP, 2006). Natural resources such as oil, gas, salt and aggregates are extracted from shelf seas, and shipping provides transport links throughout the world. It is likely that future climate change and coastal development will affect the shelf seas, although, despite numerous studies, estimating how the shelf seas will respond to future change remains highly challenging.

It is expected that future climate change will bring its own additional pressures on the coastal zone, including sea level rise and a growing interest in renewable energy schemes such as free stream tidal power. Furthermore, increasing populations require more space and reclaiming land from the sea is becoming a highly viable option (e.g. Holt et al., 2010).

According to the Foresite report commissioned by Sir David King (the UK government chief science advisor in 2000-2007) in 2004 the UK spent an annual budget of approximately £800 million on coastal defence schemes and this is estimated to increase (report available at: http://www.bis.gov.uk/foresight/our-work/projects/published-projects/flood-and-coastal-defence/general-reports). The success of coastal developments and sea defences depends upon the ability to predict high water levels. The tides make a significant contribution to high water levels and thus it is vitally important to be able to predict any changes in regional tidal systems.

The IPCC has estimated that the global sea level is rising at approximately $1.9 \, \text{mm yr}^{-1}$ (Denman et al., 2007), but it has been suggested that this is a 'lower end' estimate and a realistic value may be far higher (Rahmstorf, 2007; Nicholls et al., 2011b). Furthermore, sea level
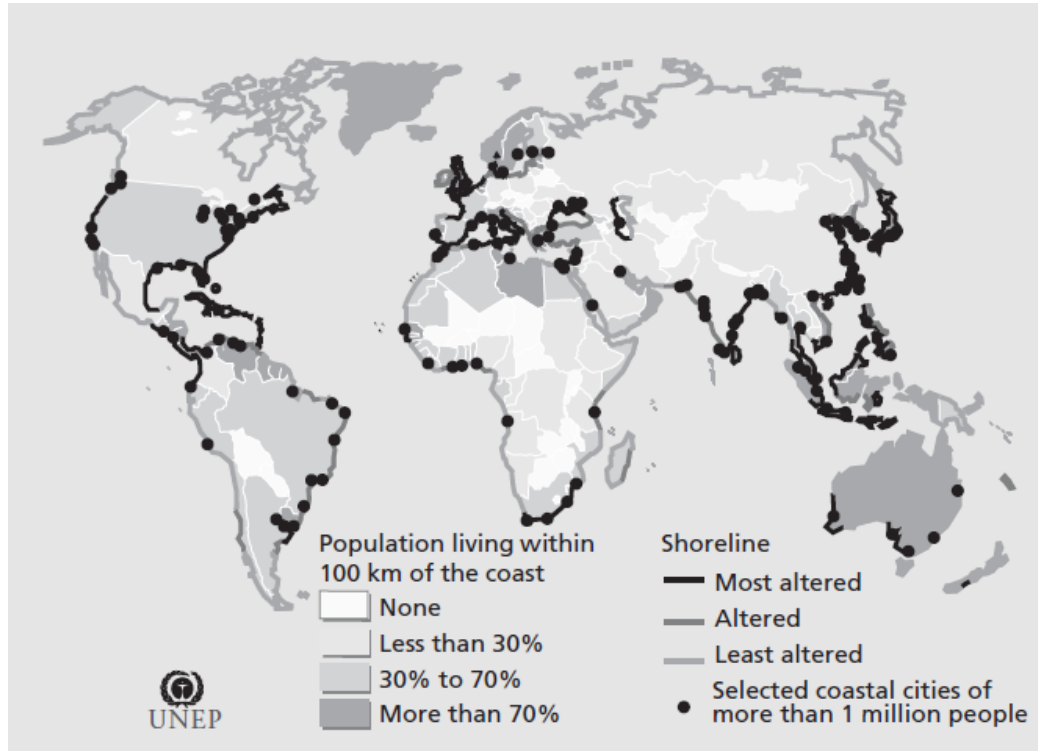
Figure 1.1: Coastal populations and shoreline change (Creel, 2003)

rise (SLR) is expected to accelerate over the century (Church and White, 2006, 2011; Woodworth et al., 2011). Studies show that the moderate SLR the ocean has experienced over the last few decades (a fraction of a meter) has already had an impact on regional tidal systems (e.g Woodworth et al., 2009; Muller et al., 2011), and future SLR may continue to have tidal impacts (Pickering et al., 2012; Ward et al., 2012).

The connection between the burning of fossil fuels and global climate change is becoming more established within society and this together with fears of energy security (and over dependence on imported hydrocarbons) have ensured the feasibility of renewable energy is becoming more important. Worldwide potential of renewable energy is estimated at approximately $500 - 1000$ TWh yr^{-1} (SDC, 2007), and tidal power has been identified as a highly predictable, economically viable, renewable energy, with technology currently available to begin the exploitation of this sustainable resource. However, while the technology and knowledge is well established to identify suitable locations to build tidal power plants (TPP), establishing and quantifying the possible local and regional effects of tidal

power plants on the tidal regime is less well known.

As the population of coastal areas has increased demand on coastal land has also risen, leading to large scale anthropogenic land reclamation and shoreline change (Fig. 1.1). For example the Netherlands has undergone significant land reclamation over the past 100 years and at present reclaimed land makes up 1/6 of the country. Furthermore, in the Bohai Sea (China) the land reclamation which has taken place during the last decade shifted the shoreline of the Tianjing port seaward more than 10 km (Paper III). Land use changes, such as the damming of rivers, has lead to increased sediment deposition and caused the growth of river deltas. Diversion of the course of the Yellow River associated with the oil-field exploration also modified the coastline along the south western Bohai Sea by about 20 km in 30 years (Paper III). It is very likely that changes in the position of the coastline will have tidal effects (e.g. Hollebrandse, 2005).

The innate predictability of the tides has been a well known oceanographic phenomena for centuries. However, it is with the advent of satellite altimetry and decades of tidal gauge data, that any deviation of the tides from equilibrium can be observed on different spatial and temporal scales. Furthermore, recent advances in tidal modelling allows high resolution of barotropic processes (i.e. processes whereby the density change is only a function of pressure, or the fluid is homogeneous in terms of density) from global to basin scale with increasing accuracy.

Historically it has been assumed that the pattern of the tides, and thus tidal amplitudes, are constant over recent time (Darwin, 1899). Therefore, when analysing high water levels (over decal to centennial scales) the tidal component has to some extent been ignored. However, recent observational studies have begun to question this premise (see e.g. Woodworth et al., 2009; Muller et al., 2011). To date, however there has been little study of how the tides may respond to sea level rise, tidal power plants and coastal developments, or a combination of the above in the future or why they do so.

The aim of this thesis is therefore to investigate the impact on regional tidal systems to change on a decal to centennial time scale in response to sea level rise, the introduction of free stream tidal power plants, and land reclamation.

We draw on the principle of Occam's Razor[1] in an attempt identify controlling processes and mechanisms that have lead to the changes observed in the hope that we can further our

---

[1]The principle that states the simplest solution, which utilizes the fewest assumptions is probably correct

understanding of regional tidal dynamics and advise the next generation of tidal models, through highlighting significant processes.

The study is limited to tidal processes only. We employ 2D (depth averaged) models and do not attempt to investigate baroclinic factors (i.e. processes that deal with density dependant processes, for example stratification). There are a number of 2D tidal models available which would be adequate for this study and we have used two: OTIS and KUTM (these models are described in detail by (Egbert et al., 2004) and (Uehara et al., 2006), respectively. See also chapter 3 and papers I-IV). We have thus chosen state of the art tidal models that are well established and validated and also accessible, allowing easy manipulation of the code. Simulations concentrate on mean sea level rise, which ignores any isostatic impact (i.e. the vertical movement of land resulting from the past loading of glaciers). Isostatic (or relative) sea level change will, no doubt, have additional effects on some regional tidal systems (including the ones we study here), but we leave this for a future study.

We have concentrated on three contrasting geographical areas; the European Shelf (Papers I and IV), the Gulf of Maine (Paper II) and the Bohai Sea (Paper III). These regional shelf seas vary significantly with respect to bathymetry, open ocean forcing and domain size. This diversity increases the likelihood of the occurrence of different processes and mechanisms in which to study.

The primary expected outcome from this project is to identify the mechanisms that control the response of regional tidal systems to SLR, TPP and land reclamation and how best to capture these changes with a tidal model. The significance of this outcome falls into two main categories. On a theoretical level we hope to increase our understanding of tidal systems by using SLR, TPP and land reclamations as additional forcing parameters and relate any tidal responses, where possible, to classical analytical wave theory. This is an attempt to generalize our results in the hope that they made be applicable elsewhere (geographically). On a more practical level we hope that any knowledge gained here can be used to improve current tidal modelling efforts and increase the accuracy of future tidal predictions, with clear implications for government policy. A secondary outcome (and a pre-cursor to the success of the primary outcome) results from the need to validate and assess our modelling efforts. Analysis of the tidal gauge network and utilization of data assimilation model products (e.g., OTIS ATLAS) will provide a benchmark to compare our model results and insight may also be gained from the observations themselves.

The original contribution to knowledge of this thesis lies primarily in the analysis of the effect of SLR on regional tidal dynamics. The process of flooding has not generally been recognized as a contributing factor to the response of tides to SLR (Pickering et al., 2012; Ward et al., 2012), but this thesis shows it to be highly significant. These results are likely to have implications to the building of flood defence systems and coastal zone development. Other areas of original contribution lie in the analysis of the effect of a combination of SLR and other processes (TPP and land reclamation) on regional tidal dynamics.

This thesis consists of a collection of background material (part 1), a summary (Part 2) which sets the scene for the four appended papers (Part 3). Part 1 includes an over view of tidal and tidal modelling theory (chapter 2), chapter 3 describes the methodology (including model descriptions). Chapter 4 describes a series of validation and sensitivity tests, designed to test the model and enable the most relevant model set up to be employed in each region and the main results from the thesis, and papers from part 3 are discussed in context with relevant literature in Part 2. Part 2 ends with a discussion and recommendations for further work in Chapter 6.

2 Tidal Theory

Broadly speaking the tides are generated by the rotation of the Earth within the gravitational pull of the moon and to a lesser extent the sun. Newton's law of gravity states that "any body of mass will exert a force of attraction on other bodies around it. The strength of this force is proportional to the product of the masses of the two bodies and inversely proportional to the distance between their centres of mass squared". This results in a varying force over the Earth's surface, stronger closest to the moon and weaker further away. However, if this was the only process the sun would be 177 time more dominant than the moon (Baker, 1991) but it is well known that the moon is the principal influence.

A standard method (termed the equilibrium model) used to help simplify this problem is to imagine a frictionless Earth without land masses and covered in one ocean of uniform depth (i.e., a Water World). The Earth-Moon system rotate about their combined centre of mass (Fig. 2.1; point B), the Earth rotates eccentrically in such a way that all points on the Earth describe the same ellipsoid, this results in the same centrifugal force experienced at every point on the Earth's surface (Fig. 2.1; green arrows). Figure 2.1 shows the gravitational force of the moon (Fig. 2.1; black arrows) and the centrifugal force (Fig. 2.1; green arrows), the equilibrium tidal force is shown as thick yellow arrows (Fig. 2.1). The vertical component of this force can be neglected as it is small when compared to gravity. Thus the tidal producing force or tractive forces is made up of the horizontal components. These are also small but of the same order of magnitude as other horizontal forces experienced in the ocean. The tide generating force over the whole globe is shown in figure 2.2 and the resultant tidal bulge formed is shown in figure 2.3.

The tide generating force at any point (other than the poles where it is zero) can be given by the force due to gravitational attraction at that point minus the centrifugal force, generated by the rotation around the systems joint centre of mass (B in Fig. 2.1) at that
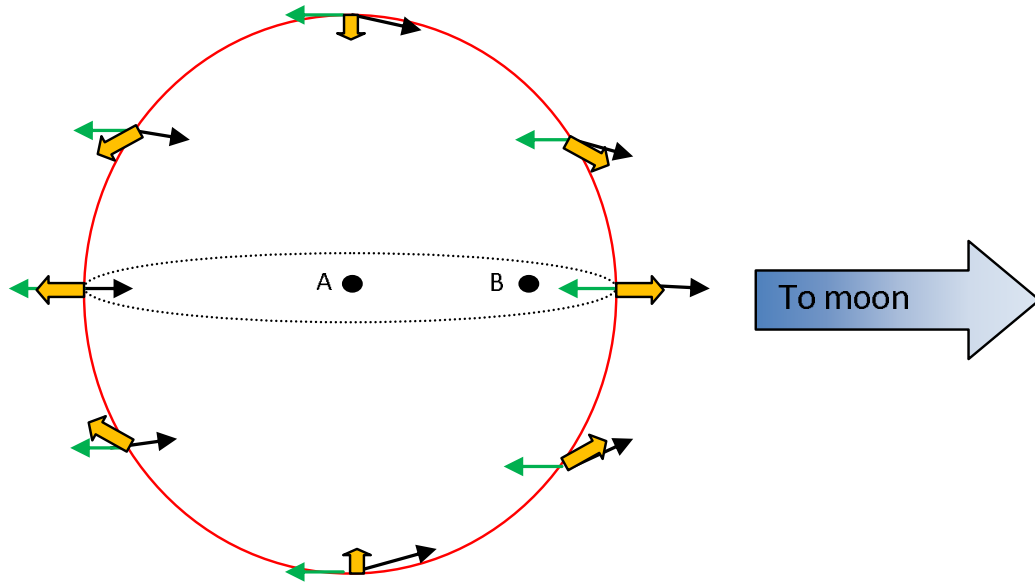
Figure 2.1: The tide generating force on a hypothetical water world. The point B is the centre of the Earth-Moon system and point A is the centre of the Earth (figure reproduced from Wright et al., 1999).

same point. If it is assumed that the orbit of the moon around the Earth is perfectly circular, the tide generating forces would be constant and result in two bulges, one on either side of the Earth (figure 2.3). As the Earth rotates a point on the Earth's surface will go through both tidal bulges, thus there would be two high tides and two low tides per lunar day. This is known as the semi diurnal (two tides per day) lunar tidal constituent. It has a period of 12.42 hours (the time it takes to complete one tidal cycle or the Earth to rotate under the Earth) and is denoted by the symbol M_2, M denoting that it is the major lunar component and $_2$ denoting the diurnal periodicity.

The moon and to a lesser extent the sun do generally have the biggest effects on tidal amplitudes, but other astronomic phenomena such as the inclination of the Earth's and sun's orbit and the angle of declination contribute constituents. Further constituents are used in the analysis of tides in shallow water (e.g. M_4 and M_8), however these are not 'real' constituents as they are not astronomically forced, but instead are generated by shallow water effects and bottom friction, e.g. M_4 (Provst, 1991). However, they are required to perform harmonic analysis. Over 600 different tidal constituents have been identified but in general only 8-16 are required for accurate tidal analysis, as for most applications, the
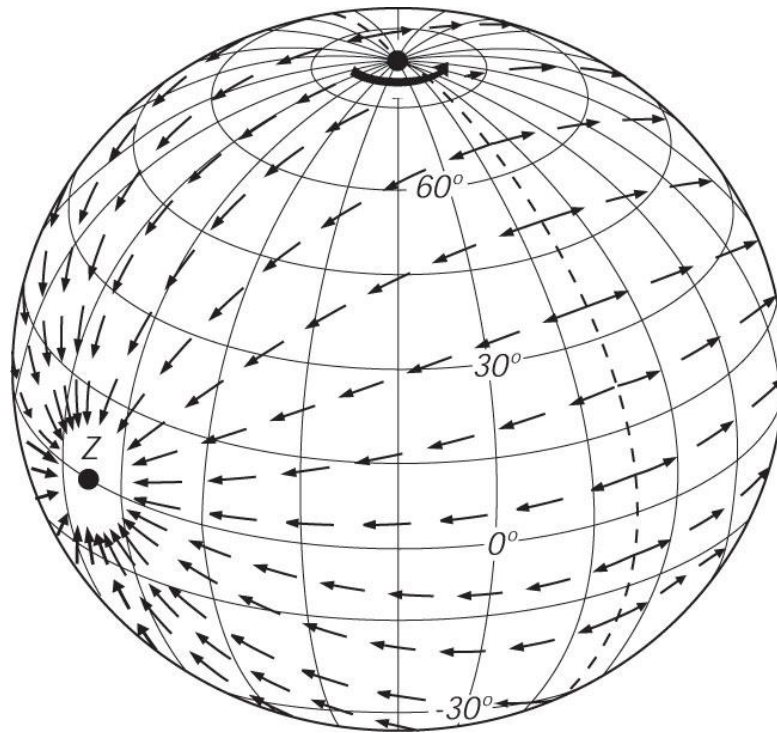
Figure 2.2: The resultant tidal generating force on the 3D Earth (figure reproduced from Stewart (2007)).
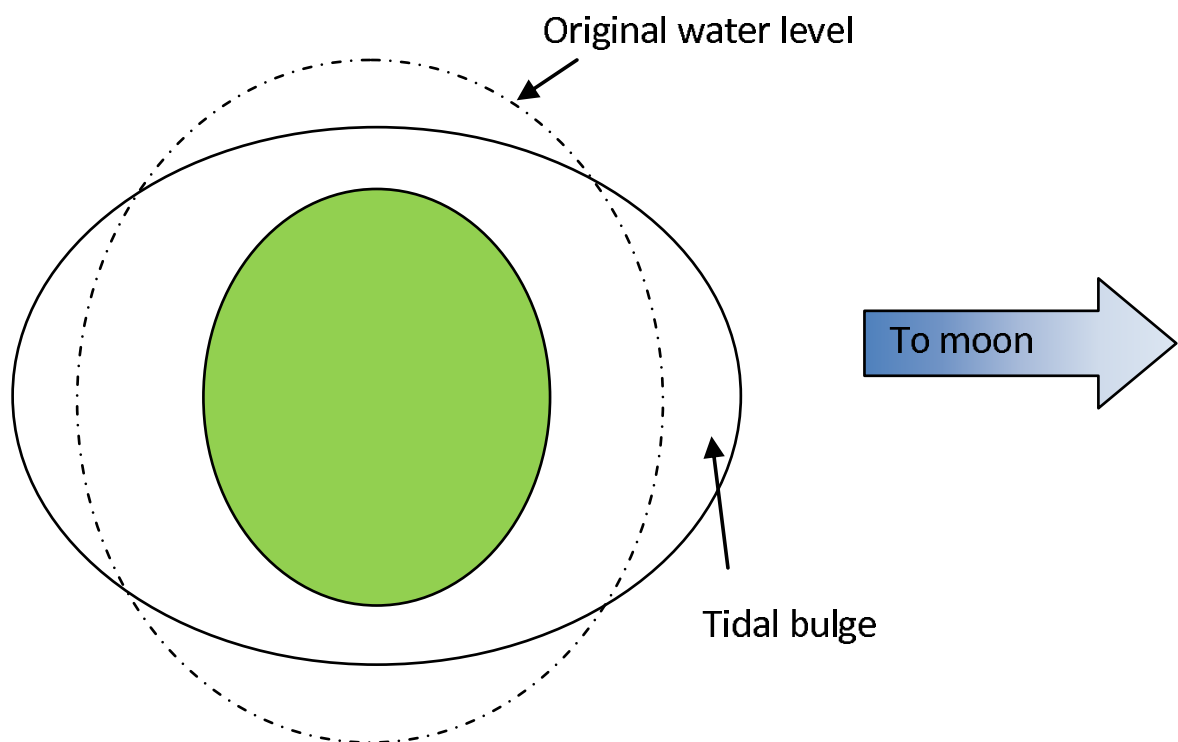
Figure 2.3: The resultant sea level on a hypothetical water world under the Earth's rotation (figure reproduced from Wright et al., 1999).

(a) Water World

(b) Flat Bottom

(c) 'real' tides

Longitude
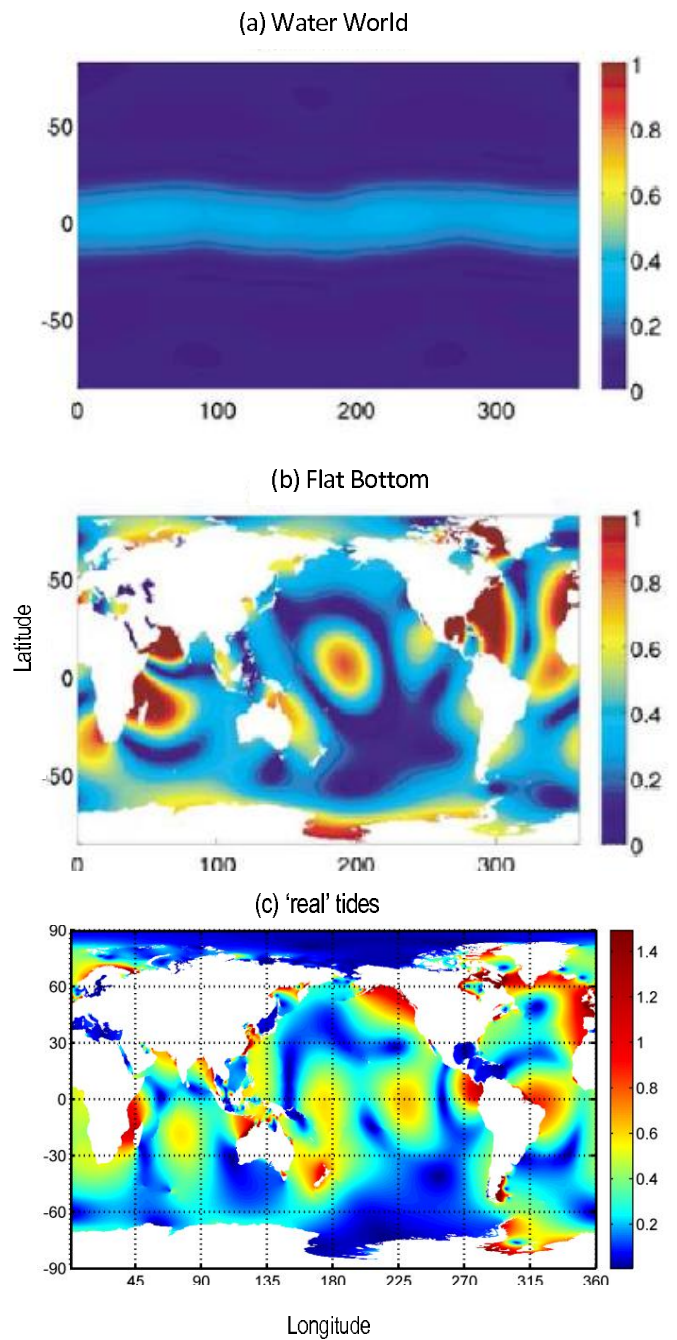
Figure 2.4: The resulting tidal amplitude (m) generated by the equilibrium tide on a hypothetical water world (a) and with continents, but no bathymetric features (b) (Arbic et al., 2009). Panel C shows the 'real' tidal amplitude (m) produced by TPOX6.2

impact of the rest are insignificant.

The effect of adding land masses only as barriers can be seen in figure 2.4. In this simulation by Arbic et al. (2009) the continents are added in to Water World, but the water depth is set to a spatially uniform value of 4000m. The presence of these land masses enhance the open-ocean tidal amplitudes by enabling resonance and topographic effects to occur. Tidal resonance amplifies the tidal amplitude and will occur when the tidal frequency is the same as, or a multiple of the natural resonance of oscillation of the basin (and discussed further in the following section).

The addition of topography also decreases the water depth around the coastal areas (adding shelf seas). This has two main effects: firstly it will decreasing the speed of the tidal wave; $C = \sqrt{gH}$, where g is the acceleration due to gravity and H is the water depth. Furthermore shallow seas dissipate more tidal energy because the velocities will be larger in shallow water than in deep water (tidal energy dissipation is discussed further in the following section). Further effects are the result of Coriolis which acts to deflect the tidal wave and rotate around a basin. This results in the formation of points of no (tidal) elevation known as amphidromic points.

2.1   Tidal energy dissipation and dynamics

The slowing of the Earth's rotation and related movement of the moon into a higher (and slower) orbit is due to gravitational torque between the Earth and moon. This torque has been attributed to tidal friction (Munk and MacDonald, 1960). The associated lunar tidal dissipation is related to the moon's orbital velocity and mass. Some of the first estimates of the moon's orbital velocity were made using Babylonian observations of the variation in longitude of where an eclipse is observed. This gave ranges of $-27" - -79"/c^2$ which corresponded to a dissipation of 1.4 TW (Jeffreys, 1920). However, this is somewhat on the low side and issues with using historic astronomic data are highlighted by Munk (1997): "Since the study of ancient observations requires competency in both astronomy and antiquities, the field has never been over crowed". More accurate values of the moons movement obtained by telescopic data were used by Munk and MacDonald (1960). These estimates were later confirmed with the development of retroreflective arrays and a process of bouncing laser beams off these reflectors in order to make highly accurate measurements of distance (Lunar Laser Ranging (LLR)). This allowed the rate of the moons recession

from the Earth to be measured as 3.82 ± 0.07cm/yr which corresponds to a dissipation of 2.5 ± 0.1TW (Dickey, 1994). Furthermore tidal energy dissipation can be computed directly using satellite alimentary adjusted tidal models (e.g. Ray et al., 1996; Egbert and Ray, 2001, and see Fig. 2.8). However there is one significant issue with this approach, assuming a constant lunar recession rate this would make the moon only 1-2 Gyr old, thus suggesting that tidal energy dissipation was significantly smaller in the past (Green and Huber, 2013a).

While the total energy dissipated is well known (for the present day at least), the spatial distribution of tidal energy dissipation has proven to be a far more complex problem (see Munk, 1997, for a review). It was originally thought that almost all of the global tidal energy dissipation takes place in the bottom boundary layer (BBL) (Taylor, 1919; Jeffreys, 1920; Miller, 1966), which suggests 99% of the ocean area accounts for 1% of the tidal dissipation (Munk and Wunch, 1998). The likelihood of such a high percentage of the global tidal energy dissipating in BBL has been questioned (see Munk, 1997, for a review) and shown to be wrong (Egbert and Ray, 2000).

Internal waves of tidal frequencies (internal tides) have long been observed but their contribution in the dissipation of the surface tide has remained elusive for some time (Munk, 1997; Garrett, 2003). The large amplitudes of internal tides ensure that they could not be generated by tidal potential alone (see for example Munk, 1997; Munk and Wunch, 1998) and require topographic features to generate the conversion from barotropic to baroclinic modes (e.g. Green and Nycander, 2013, for a review of conversion schemes). While some of the early calculations suggest that the energy dissipation from the generation of internal waves is negligible (e.g. Baines, 1982), more recent mapping of the spatial distribution of tidal energy inferred from satellite altimetry and inverse modelling, Egbert and Ray (2000, 2001) found that $25 - 30\%$ of the M_2 global tidal energy dissipates in the open ocean. However while this method did show that tidal energy dissipation was enhanced over rough or steep topography, it did not identify the contribution from internal wave generation (as opposed to other mechanisms) and thus direct measurements are necessary. Some of the early direct calculations found that significant tidal energy could be dissipated through the conversion to baroclinic modes in the open ocean (Sjï¿½berg and Stigebrandt, 1992; Gustafsson, 2001). However these solutions were found not to converge at high resolutions (Laurent and Garrett, 2002). Access to high resolution global bathymetric databases and increased computational power has furthered the field almost

as a by-product of the development of improved tidal solutions (Arbic et al., 2004; Egbert et al., 2004). In these tidal models (see for example Egbert et al., 2004; Uehara et al., 2006) the tidal conversion is parametrized as an additional frictional term (e.g. Jayne and l.C. Laurent, 2001; Nycander, 2005; Zaron and Egbert, 2006). Both Egbert et al. (2004) and Green and Nycander (2013) have tested a number of these parametrizations in a global tidal models with and without assimilation. Both studies showed all parametrizations tested produced similar total global conversion rates (with the exception of the parametrization by Baines (1982)), but Green and Nycander (2013) show that the geographical distribution of the conversion varied significantly.

Changing the spatial (and temporal; (see for example Pugh, 1981; Muller et al., 2011)) distribution of tidal energy dissipation in a region or basin can have significant impacts on the tidal dynamics (e.g. Hendershott and Speranza, 1971). This is evident in tidal simulations which include tidal energy power plants and effectively remove energy from the tide (paper II; see also chapter 5.2). Furthermore, changing a basin's shape by land reclamation or flooding can significantly alter the spatial distribution of tidal energy dissipation and therefore the tidal dynamics (papers I and III).

2.1.1 Tides in shelf seas

While the open ocean tides are generated by the differing tidal potential (and resulting tide generating force) across the ocean, tides on the shelf seas are driven by the rise and fall of the ocean tides at the shelf break (Taylor, 1919). The main effect of moving from the deep ocean onto the continental shelf is a decrease in wave speed and an increase in the tidal amplitude, due to the decrease in water depth (Pugh, 1996). Although, some of the energy will be reflected (Taylor, 1919; Pugh, 1996) the tidal amplitudes and currents will tend to be stronger in the shelf seas compared to the deep ocean. A popular method of describing a tidal regime pictorially is the co-tidal chart (see Fig. 2.5 and 2.6). In these type of schematic the phase of the tide is plotted as contour lines showing the direction and path of the tidal wave.

A Kelvin wave in the ocean is a wave that is produced when the Earth's Coriolis force is balance by the presence of a land mass. They are no-dispersive and propagate with the coastline to the right in the Northern hemisphere. Taylor (1921) investigated a problem whereby a rotating, semi-enclosed, rectangular basin is forced at one end by a Kelvin wave. The wave is allowed to propagate through the basin and reflect at the closed end (Fig. 2.5).

Figure 2.5: Co-tidal plot of a reflected Kelvin wave (with no energy loss) in a rectangular basin (Taylor, 1921)

The analytical solution is a superimposition of the incoming wave, reflected wave and any Poncaré waves created, and a solution is readily available. There have been a number of further studies that have explored and extended this problem; Hendershott and Speranza (1971) have simulated energy dissipation at the far end of an idealized channel, Rienecker and Teubner (1980) and Rizal (2002) have increased bottom friction and Brown (1987, 1989) investigates a situation whereby an oscillating boundary is present at the closed end of the channel. There has also been a number of studies that have investigated the impact of bathymetry on the Taylor problem (Roos et al., 2011). These studies suggest that the shape of the North Sea is very important to it's tidal regime. In the Irish Sea Pugh (1981) investigated the effect of the spring-neap cycle on the position of an amphidromic point in St Georges Channel and found that the changes in tidal energy dissipation associated with the different states of the spring-neap cycle caused the movement of the amphidromic point on to and off of the Irish mainland.

The tides in the North Sea essentially behave like a Kelvin wave. The wave enters from the North Atlantic and propagates along the UK coast. It is then reflected at the end of the basin along the Dutch coast. The reflected wave then travels back along the coast of continental Europe. This phenomenon can be investigated using a problem proposed by
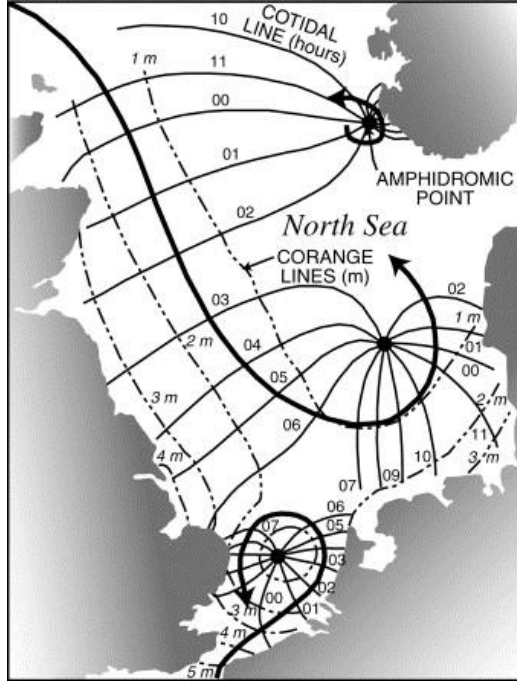
Figure 2.6: Co-tidal plot of the diurnal tidal regime in the North Sea (Kvale, 2006). Arrows show the direction of the tidal currents.

Taylor (1921) and subsequently used by e.g. Roos et al. (2011), Hendershott and Speranza (1971) and Brown (1987) to investigate the tides in the North Sea.

Paper I shows that the flooding of the Netherlands associated with sea level rise and the large areas of shallow water that creates, causes increased dissipation of tidal energy. This causes the eastward movement of the second amphidromic point (if we assume the top one is number one and the bottom one is number three) in the North Sea and is analytically described by the idealized scenario in Hendershott and Speranza (1971).

Tidal resonance is caused by the forcing and the natural frequency of the system being the same or close. The natural frequency is largely influenced by water depth and basin dimensions. Tidal resonance creates tides that are larger than could be expected from equilibrium tidal theory and allows the particularly high tidal range seen in the Severn Estuary (Fong and Heaps, 1978) and the Bay of Fundy (Garrett, 1972) and occurs when:

$$L = \frac{\sqrt{gH}}{4}T \tag{2.1}$$

Here L is the length of the basin, g is the gravitational constant, H is the water depth
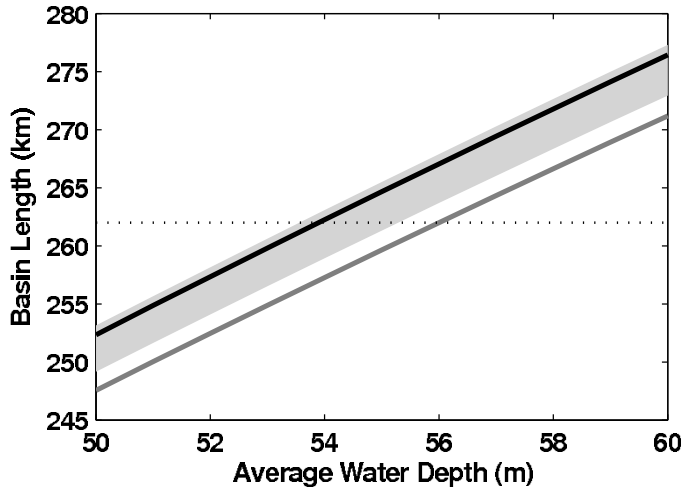
Figure 2.7: Necessary basin length (L) as a function of average water depth for tidal resonance to occur from Eq. (2.1) in the Bay of Fundy. The grey and black lines show the basin length and average water depth combination in Eq. (2.1) which gives resonance for N_2 (black line) and M_2 (grey line). The estimated natural frequencies as estimated by Godin (1988) are shown as the grey patch. The horizontal dotted line shows the length of the basin in the present day bathymetric database used for the numerical simulation (From Paper II).

and T is the period of the tidal constituent under investigation. In Fig. 2.7 the tidal period is plotted as a function of basin length and average water depth for the Bay of Fundy and the Gulf of Maine (Paper II). The present day resonant period of the Bay of Fundy lies between 12.5 and 13.4 hours (Garret, 1972; Greenberg, 1979; Godin, 1988, 1993; Ku et al., 1985, and depicted by the shaded are in Fig. 2.1), which is close to the periods of the N_2 (12.66 hr) and M_2 (12.42 hr) tidal constituents (shown by the lines in Fig. 2.7). This would suggest that the tides of the Bay of Fundy are highly sensitive to any impact that would change the resonance qualities of the basin (e.g. basin shape, length or water depth).

In Paper II we see that the basin is approaching resonance with increasing sea level or water depth (assuming no flooding takes place). Furthermore by substituting the average water depth of the Bay of Fundy plus the SLR required to reach resonance in to Eq. (2.1) (from the no flood runs, 16 m) a natural resonant period for the Bay of Fundy of 11.2 hr was estimated (Paper II).

2.2   A brief history of tidal modeling

Although harmonic analysis of observed sea-level has allowed the accurate prediction of coastal tides for hundreds of years, it is the advent of satellite altimetry and global, high-resolution tidal modeling that has allowed predictions of coastal and open ocean tides with the accuracy of a few centimetres (Egbert and Ray, 2000, 2001, 2003; Egbert et al., 2004). Tidal models are generally based on the shallow water equations. As there is no general solution to the equations of motion, physically relevant simplifications and approximations are made. This is where most of the variability between different tidal models lies, how individual processes described in the shallow water equations are parametrized.

While global tidal modeling began in the late 1960s (with break through in the 1970s regarding the handling of ocean self attraction and loading (SAL) (Hendershott, 1972), results were qualitatively realistic, but not accurate enough for practical tidal predictions (LeProvost et al., 1994). This led to the development of a series of semi-empirical models that used the assimilation of tidal gauge data to constrain the model equations. A lack of computational power could be blamed for the delay in the development of an accurate tidal model free from data assimilation, as the main issues appears to be the inability to correctly simulate the dissipation of energy. As two thirds of the tidal energy is dissipated in shallow, coastal areas (Ray et al., 1996) through bottom boundary shear, it is imperative that these coastal regions are resolved and this required a resolution of the order of 10km.

The main break though came when LeProvost et al. (1994) developed a global finite-element model, and this heralded an new era in numerical models, showing that the global tides can be modelled accurately in a purely dynamical way only forced by astronomical tidal potential (see section 2). There where however issues with LeProvost's first model, they calculated solutions for each ocean basin individually and then knitted them together allowing the boundary conditions between each ocean basin to regulate the results so that they give the best agreement to tidal gauges (Lyard and Genco, 1994). Thus the model was not truly 'free' from data assimilation.

The advent of TOPEX/Poseidon altimetry data allowed greater assimilation within tidal models, but the high accuracy observations of the open ocean showed discrepancies in the current tidal models of the time, including a significant dissipation of tidal energy in the open ocean, that was not predicted in the models (Egbert and Ray, 2000). Egbert and Ray (2001) empirically mapped the global tidal energy dissipation from TOPEX/Poseidon

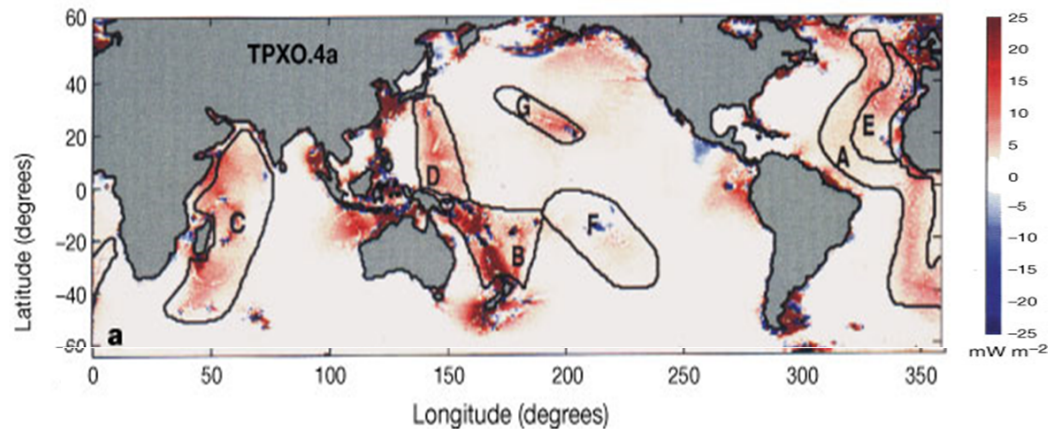Figure 2.8: The location of energy dissipated from the tide (Egbert and Ray, 2000). Additional labels are from the original paper and are not discussed further here.

satellite altimetry data. This dissipation is suspected to be due to the conversion of baroclinic waves to barotropic and is extremely localized to 'hot spots' of rough topography in the open ocean (Egbert and Ray, 2001) (see fig. 2.8).

3 Methodology

This thesis is predominantly based on the results from model simulations of two tidal models, KUTM and OTIS. The use of two models allows flexibility when designing practical applications and numerical experiments. Tide gauge and satellite altimetry products have been used to validate and force the models. This chapter describes the two tidal models used, how they were set-up for the different studies and a description of the observational data used.

3.1 Tidal Modelling

Both the tidal models are 2D and solve the shallow water equations. OTIS solves the depth integrated form, given by:

$$\partial U/\partial t + f \times \mathbf{U} + \mathbf{U} \cdot \nabla \mathbf{u} = -gH\nabla(\eta - \eta_{SAL}) - \mathbf{F} + k\nabla^2 \mathbf{U} \tag{3.1}$$

$$\partial \eta/\partial t = -\nabla \cdot \mathbf{U} \tag{3.2}$$

Here $\mathbf{U} = \mathbf{u}H$ is the depth-integrated volume transport given by the velocity $\mathbf{u}$ times the water depth H, t is time, f is the Coriolis vector, η and η_{SAL} is the tidal elevation and self attraction and loading (SAL) elevation, respectively, $\mathbf{F}$ is the dissipative stress from bed friction and $k\nabla^2 \mathbf{U}$ is a crude parametrization of horizontal turbulent eddy viscosity, where k is the horizontal eddy viscosity coefficient.

A form of OTIS is available that solves the linearised equations of motion (removing all non-linear advective terms) and therefore also neglects horizontal turbulent eddy viscosity. While it could be argued this is valid in the deep ocean (Egbert et al., 2004), including the

non-linear terms increased the accuracy of the model in the regional setting we use here. As the linearised version of the model is not used in the thesis, it is not discussed further.

KUTM is formulated slightly differently and solves a depth averaged form of the shallow water equations, where $\mathbf{u}$ is the depth averaged velocity:

$$\partial H\mathbf{u}/\partial t + f \times H\mathbf{u} + (\mathbf{u} \cdot \nabla)D\mathbf{u} = -gH\nabla\eta - \mathbf{F} + k\nabla^2\mathbf{u} \qquad (3.3)$$

$$\partial\eta/\partial t = -\nabla \cdot (D\mathbf{u}) \qquad (3.4)$$

In these equations the processes of SAL is not included (see below for a further discussion).

The dissipation from bed friction is formulated using a standard quadratic bed friction formulation. So for OTIS this would be:

$$\mathbf{F} = C_d\mathbf{U}|\mathbf{u}|/H \qquad (3.5)$$

and for KUTM:

$$\mathbf{F} = C_d\mathbf{u}|\mathbf{u}| \qquad (3.6)$$

Where C_d is the bottom friction coefficient. C_d is a tunable factor, i.e., the model is run using a variety of different values for C_d and compared to observations in order to get the value that produces the most accurate results.

Both models use a finite differencing schemes to solve the shallow water equations (Eqs 3.1–3.4) on an Awaraka C grid with no data assimilation (Egbert et al., 2004; Uehara et al., 2006). The non-linear terms associated with finite element schemes place high demands on computational power (Dyke, 2001). Thus finite differencing schemes appear to be more popular in tidal modeling than finite element schemes (Dyke, 2001). An Awaraka B grids works well for course resolution models (Miller, 2007). But the Awaraka C grid has the advantage that all variables are calculated at different positions, with the u velocity points positioned to the east and west of the elevation and v velocities positioned to the north and south of the elevation points. As in this application we have a varying bathymetry as well as elevation (i.e varying water depth) the elevation and bathymetry grids are specified at the same point in the centre of the cell and are defined as an average over each grid

cell. u and v velocities or volume transports are defined at the edges of the cells and are defined as an average over the cell edge.

Both models are regional and thus need to be 'forced' at the outer boundary of the computational domain to put the simulation in to a global context. The standard set-up for each model has slightly different requirements for the boundary conditions. OTIS uses elevation, whereas KUTM takes both elevation and velocity, but velocity is the primary consideration. A no-flow condition is implemented in both models at the coastline. It is important to note that the boundary conditions remain the same for each perturbation simulation (e.g. SLR, TPP etc), although they are of course different for each region. This makes the assumption that the effect of the perturbation on the shelf does not impact the global tides. Generally this is valid as the impacts of the perturbations are shelf bound, although sensitivity runs have been made to test the potential implications of this (see section 4.3).

The free surface elevation caused by the tides results in a deformation of the sea floor due to the varying weight of the water column (Hendershott, 1972). This redistribution of mass over the Earth's surface results in an effect on the Earth's gravity field which in turn feeds back on the tidal dynamics and is termed 'self attraction and loading (SAL)'. The solution is equally not trivial and requires the global integration of the tidal elevations (or bottom pressure). Instead, SAL can be approximated using an irritative solution, making it less computationally expensive. The broad scale mapping of tidal features (LeProvost et al., 1994) and later Topex and Posiden (Egbert and Erofeeva, 2002) allows a reasonably accurate initial estimation of tidal elevations due to SAL (Ray, 1998) and a bootstrap method can be used to compute SAL and added to the shallow water equations. However Egbert et al. (2004) pointed out that these solutions use data assimilation and therefore not independent.

Scalar approximations have been suggested to reduce the computational power required and iterations needed. Accad and Perekis (1978) approximated a scaling relationship of 0.085 and Schwiderski (1978) suggested 0.1 to the local tidal elevation in the form;

$$\eta_{SAL} = \beta\eta \tag{3.7}$$

where β is 0.085. This approximation has been shown to reduce the error with not including SAL by approximately 30% (Stepanov and Hughes, 2004). This is the method used in this project for simulations made by OTIS (with $\beta = 0.09$), while KUTM does not include

Constituent	Frequency (cph)	Simulation time required (hrs)
(M_2)	0.0805	13
(S_2)	0.0833	355
(N_2)	0.0790	662
(K_1)	0.0418	24
(O_1)	0.0387	328

Table 3.1: Time (hrs) necessary to prevent interference from neighbouring tidal frequency bands whilst conducting harmonic analysis (Emery and Thomson, 2001).

SAL. This approach is valid as the areas of interest are small, however a more rigorous application would be required for a global simulation (Arbic et al., 2004).

The run time of the model is user defined and dependent on two considerations; time needed for model spin up and harmonic analysis. Both models require a period of time at the start of the simulation, where the model is spun up. This is the time taken for the model to reach geostrophic equilibrium, from initial conditions, under the forcing from the boundary conditions. Tidal models generally do not take as long as full circulation models (Kantha and Clayson, 2000) as barotropic waves travel faster than Rossby-type waves. In the following project spin up times in the order of 10 days have been used, the difference between the different times used is model and domain dependent.

The simulation time needed for harmonic analysis is dependent on the constituents simulated. In the first instance it is necessary for the period simulated to be long compared to the periods of the tidal constituents concerned. If only M_2 is considered the simulation needs to be at least as long as one tidal cycle, so ≈ 13 hrs. However this will increase when it becomes necessary to simulate more than one constituent. In this instance the simulation time needs to be long enough to distinguish between constituents with similar frequencies, for example to distinguish between M_2 and N_2 signals a simulation time of at least 28 days is needed (see table 3.1; Emery and Thomson (2001)). If the simulation time is not long enough signals from neighbouring constituents in the frequency band will interfere with the analysis. Table 3.1 gives the simulation time (just for harmonic analysis, i.e. not including spin up) required to distinguish between the signal from each constituent.

3.1.1   KUTM

The Kyushu University Tidal Model (KUTM) is described by Uehara et al. (2006) and has been used several times for simulations on the European Shelf (Uehara et al., 2006; Ward et al., 2012, paper I), the Bohai Sea (Paper III) and a previous version of the model has been used for the Yellow Sea (Uehara and Saito, 2003). The model is forced at the open boundaries by surface elevation and tidal velocities prescribed from, e.g., the TPXO database or from another model source. The bathymetric and boundary forces are totally user dependent, with no default predefined. In its original state the model does not include tidal conversion, ocean self attraction and loading, or wetting and drying. However, parametrization of these processes were added, when required, throughout the present work. The tidal conversion was added by Holly Pelling and wetting and drying by Dr. Kastuto Uehara. Present formulations of KUTM are not parallelized, therefore computationally expensive runs will take sometime.

The main advantage of KUTM is in its simplicity and accessibility - the source code is fully accessible. Furthermore, the model domain, inputs and initial validation was already in place for paper I. The opportunity to work directly with Dr. Katsuto Uehara in Japan and to make some improvements to KUTM's code, therefore it was used for paper III. The main disadvantage of KUTM is the length of time to run a simulation, as it only runs on one processor, it is not feasible to use it for higher resolution simulations (papers II and IV).

3.1.2   OTIS

The Oregon State Tidal Inversion System (OTIS) was developed by Egbert et al. (1994, 2004) and has been used in global and regional settings (e.g. Egbert et al., 2004; Green, 2010; Green and David, 2013; Green and Huber, 2013b, papers II and IV). While the solution used here is totally independent of any data assimilation, solutions with data assimilation are available (http://volkov.oce.orst.edu/tides/atlas.html). This system is fully relocatable and can thus be used both regionally and globally. The regional model is forced at the open boundaries using tidal elevations from the TPXO database (Egbert and Erofeeva, 2002). Many processes are already implemented in the model and can be utilized at will, e.g., wetting and drying, tidal conversion (not used here). At present the model is parallelized thus computationally expensive simulations can be made relatively

quickly.

The main advantage of using OTIS is that it is fully portable with numerous pre and post processing scripts available. This made setting the model up for new areas reasonably simple. In this project the model was parallelized on to two processors making runs faster than KUTM allowing higher resolution runs to take place. However the university facility available at the beginning of the project was not as stable as the one available for KUTM.

3.1.3   Wetting and drying and flood definitions

The concept of flooding is important in this thesis, therefore it is important to define what it is and distinguish it from similar processes. In this project flooding is the permanent inundation of land due to SLR. This is similar to wetting and drying, a process that is only used in paper IV, but discussed in terms of the European Shelf in section 4.3. Wetting and drying is the parametrization of the impact of the tidal flood and ebb of the intertidal zone, whereby a number of cells flood and dry periodically during the tidal cycle. The time in which they are flooded is dependent on the tidal amplitude and water depth.

Figure 3.1 is a schematic showing the different cell definitions and how they change with sea level rise. Panels a and c show the intertidal zone where, if implemented, wetting and drying would occur. Also shown is a flood defence, which is defined in this project as walls and implemented by increasing the height of the topography at the coastline, at the top (landward boundary) of the intertidal zone. When SLR is implemented (panels c and d) the water depth increases and low level land cells become defined as water, also if wetting and drying is implemented the increased water depth over the intertidal zone will redefine some cells in the intertidal zone as water (or permanently wet) and some land cells as intertidal. Where the flood deferences are located around the whole coastline (i.e. in the no-flood runs) no land cell will change to wet cells, the water depth will increase.

This definition means that the volume of added water associated with SLR is not consistent between flood and no flood runs (there will be slightly more in the flood runs). But in order to investigate the impact of increasing water depth and flooding, this is unavoidable.

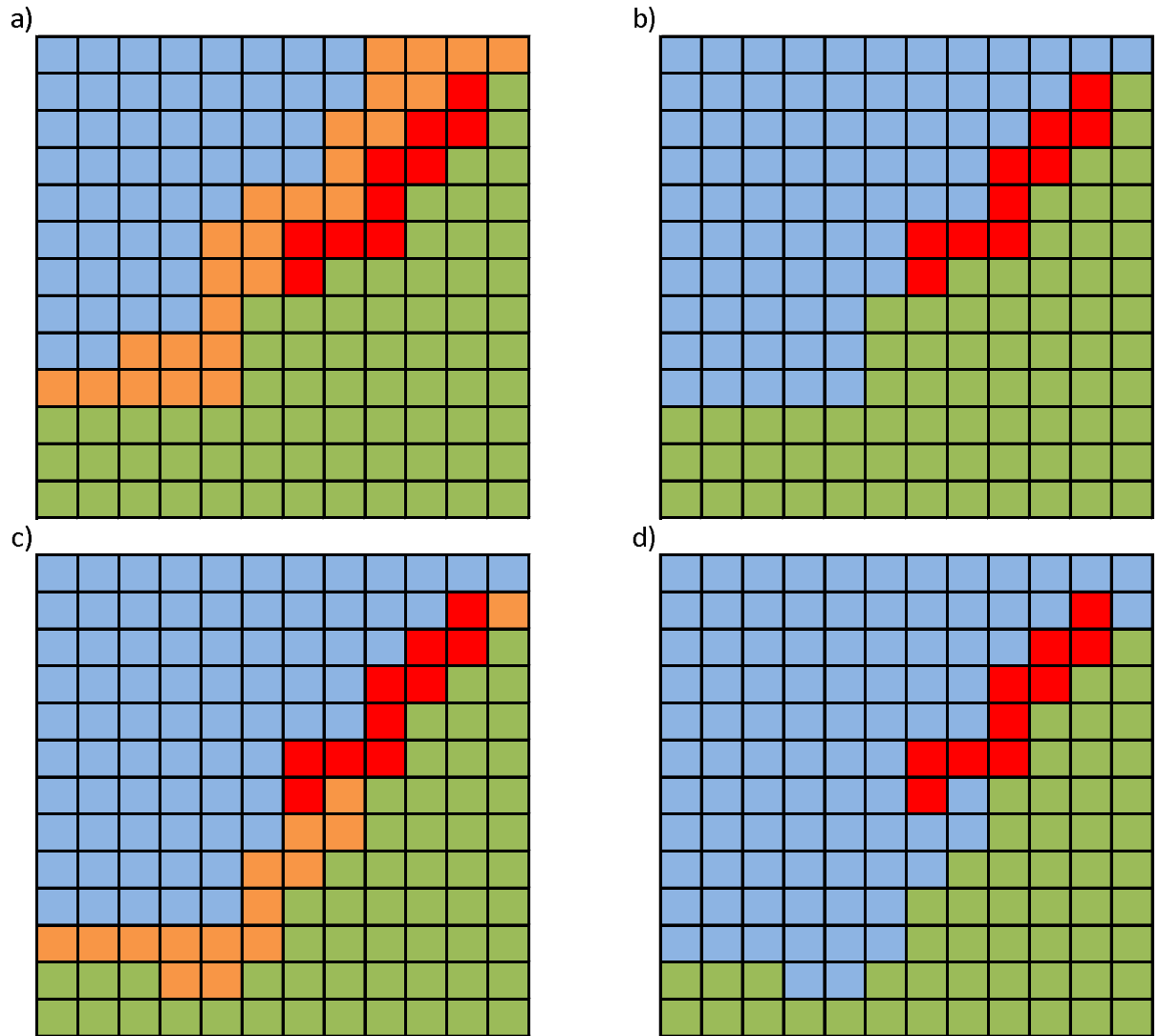Figure 3.1: A schematic showing the cell definitions and how their definition change with SLR. Green cells are land, blue cells are sea, orange cells are the intertidal zone and red cells are flood defence. Panels a and b show the present day and panels c and d show the cell definitions with SLR. Panels a and c include wetting and drying (therefore there is an intertidal zone), while panels b and d do not.

3.2 Key diagnostics

Throughout the project an number of additional parameters are computed from the model output in order to help understand why the perturbations are impacting the tidal regime in any particular way.

3.2.1 Bed shear stress

Bed shear stress is a measurement of the force of friction exerted on the sea bed by the movement of the overlaying water. It can be calculated as:

$$\tau = \rho C_d |u^2| \tag{3.8}$$

The units of bed shear stress is km m^{-3} or Nm^{-2}, which are the same units as pressure. The bed shear stress is very important when inferring sediment transport, as any transport will only occur when the bed shear stress becomes strong enough to overcome the gravitational and frictional forces holding the grains to the bed.

3.2.2 Tidal energy dissipation

Tidal energy dissipation is the measurement of the loss of kinetic energy from the tides, and ultimately to heat, by friction. In this case we are using a 2D model with no internal wave drag parametrization, therefore assume all tidal energy is dissipated through the seabed via bottom friction. The rate of dissipation is calculated using a standard expression for tidal boundary layers (see for example Kunze et al., 2002; Nash et al., 2005):

$$\varepsilon = \rho C_d |u^3| \tag{3.9}$$

Therefore, tidal energy dissipation and bed shear stress are strongly related.

3.2.3 Tidal energy flux

The tidal energy flux is useful to consider in combination with the parameters defined above, as while tidal energy dissipation shows where the tide losses its energy, tidal energy flux shows where the energy comes from and in what direction it is going. The horizontal tidal energy fluxes were calculated from the correlation between the tidal velocities ($\mathbf{u}'$) and sea level (p') perturbations:

$$E_f = \langle \mathbf{u}'p' \rangle \qquad (3.10)$$

Here the brackets denote time-averages over a suitable period (i.e. 25hrs). The perturbation in sea level and tidal velocities are calculated relative to their average. However as the time average of a single harmonic is zero, the perturbations are given by:

$$\mathbf{u}' = \mathbf{u}_o \sin(\omega t - \phi_{\mathbf{u}}) \qquad (3.11)$$

and

$$p' = \rho g \eta_o \cos(\omega t - \phi_\eta) \qquad (3.12)$$

Where η_o and $\mathbf{u}_o$ are the amplitudes of the elevation and transports of the constituent under consideration and ω is the angular frequency. $\phi_{\mathbf{u}}$ and ϕ_η the phase for the velocities and elevation respectively and t is time.

3.3   Observations

We require observational data to force and validate the tidal model solutions. These include tidal amplitude, their respective phase and tidal velocities with their respective phase. We have used observational data or data products from three sources; tidal gauge data, the TPXO database and regional high resolution simulations from the OTIS ATLAS system (http://volkov.oce.orst.edu/tides/atlas.html).

In-situ measurement of coastal sea level have been made for centuries and accurate, hourly records of sea level are available at some tide gauge stations from the 1800s. Tidal gauges measure the sea level relative to a datum or reference point, normally on land. There are a number of groups that collate and distribute research quality tidal data. For this project UK tidal gauge data was used from BODC (https://www.bodc.ac.uk/data/onlinedelivery/ntslf/) and data from the rest of the globe was obtained from the University of Hawaii Sea Level Center (UHSLC; http://uhslc.soest.hawaii.edu/data/fdd). Other data was obtained from the literature. A continuing issue with the use of tidal gauge data is the spatial availability of long-term, quality data – especially in the Southern Hemisphere (Fig. 3.2). Furthermore, due to socio-economic reasons not all countries are willing to make tidal gauge data
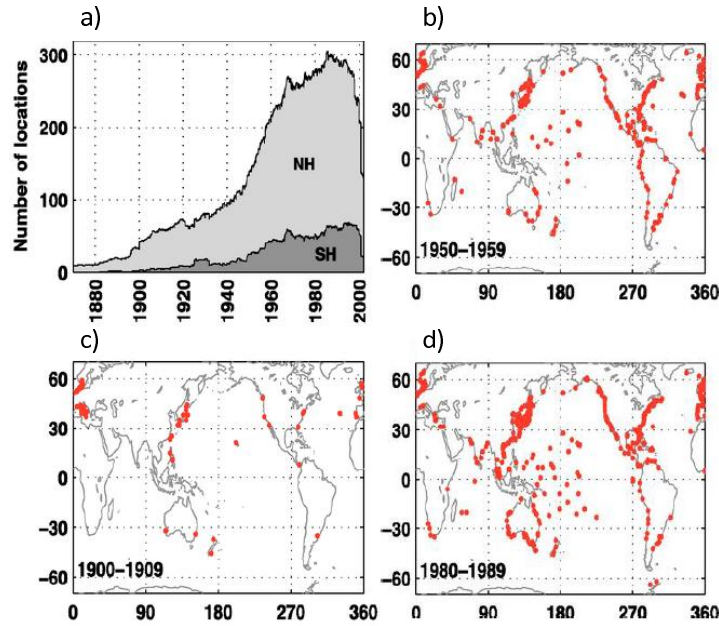
Figure 3.2: (a) The discrepancy between the number of tide gauge stations in the Northern and Southern Hemispheres (NH and SH, respectively) as a function of time. Panels (b) to (d) shows the spacial distribution of stations (red dots)(IPCC, Chp5).

available to the research community (e.g. North Korea and China; per. comm. P. Woodworth). Data can also be affected by natural land movements (including earthquakes) and the effects of riverine runoff as well as anthropogenic influences such as coastline modification and dredging (e.g. Paper III).

In this project we have used the TASK tidal analysis software (Bell et al., 1999) which uses Doodson harmonic analysis to obtain the required tidal constituents amplitudes and phases. Tide gauge data has been used to validate long term changes in tidal properties (Paper III and IV) and to validate tidal simulations for the Bohai Sea as use of OTIS ATLAS was not applicable (Paper III).

Satellite altimetry is a relatively new field of oceanography and can provide high spatial and temporal resolution, quasi-global (although concentrated over the equator) sea level data. Satellite altimetry such as TOPEX/Poseidon provide surface height measurements of

the globe between 66^oN and 66^oS with an accuracy of 4.2 cm (http://sealevel.jpl.nasa.gov/missions/topex). By applying this data and inverse solutions (i.e. work backwards from the data) to the shallow water equations high resolution tidal solutions can then be calculated. The TPXO database is an example of these solutions and is the database we have used for the boundary conditions in our model simulations. The TXPO database is a 1/4 x 1/4 degree horizontal resolution.

OTIS Atlas is an extension of the TXPO database using TXPO satellite altimetry data and the OTIS tidal model. The inverse solutions are based on the global OTIS tidal model (see chapter 3.1.2 for a further description) with significant data assimilation (tidal data from various satellite altimetry sources). A set of high resolution regional solutions are available that cover the areas discussed in this project. In this study we have used the OTIS Atlas data set to validate some of our control solutions (Papers I, II and IV). However, as the satellite data assimilated covers a period of up to 10 years it was not applicable for the validation of long term studies (Paper III).

3.4 Model set-up

We have employed various model set-ups that are specific to the particular region or study, these are summarized in table 3.2 and fully described in the attached papers:

Table 3.2: Model set-up employed for each study

Parameter	Paper I	Paper II	Paper III	Paper IV
Model	KUTM	OTIS	KUTM	OTIS
Latitude limits (deg)	45 to 65	39.5 to 46	37 to 41	45 to 65
Longitude limits (deg)	15 to -15	-71.5 to -63	118 to 122	15 to -15
Resolution (deg)	1/12	1/60	1/60	1/60
Boundary conditions	TXPO	TXPO	TXPO	TXPO
Bathymetery	Uehara 06	Composite	Navigational charts	Uehara 06/ GEBCO
Number of constituents	5	5	5	1
Run time	45	45	45	11
SAL	none	$\beta = 0.1$	none	$\beta = 0.1$
C_d	2.6×10^{-3}	3×10^{-3}	1.5×10^{-3}	2.75×10^{-3}

4 Model Validation and Sensitivity Simulations

4.1   Model validation

In order to draw any useful conclusions from our model runs we need to fully asses the model performance with realistic configurations. The accuracy of all tidal models is highly dependant on the quality of the input data, most notably bathymetry. Therefore it is necessary to validate control simulations for each study area. The model set-up is shown in section 3.4.

For this assessment we have used two main statical assessments; root mean squared error (RMSE) and variance capture. RMSE is an estimate of the difference between modelled and observed data sets:

$$RMSE = \sqrt{\frac{1}{n}\sum_{i=1}^{n}(D_i - S_i)^2} \tag{4.1}$$

Where n is the number of modelled points/observations, D_i are the modelled results and S_i are the observations. RMSE can give the average magnitude of the errors but it does not give any information on the direction of these errors (i.e. does the model over or underestimate the observations). As in Arbic et al. (2004) we computed the relative errors in the form of tidal amplitude variance capture, given as a percentage by $100 \times [1-(\bar{D}/\bar{S})^2]$, where the over-bar denotes an mean of all points. This gives an estimate of the errors in relation to the signal of the observations and calculate how well the model captures the structure of the observed field. The advantage of this calculation over RMSE is that the errors are calculated relative to the observed signal, and it is therefore possible to directly

Table 4.1: RMSE and variance capture (P) of KUTM compared to OTIS-ATLAS on the European Shelf for tidal amplitude (m) and tidal current velocity (m s^{-1}), data from paper I

Property	M_2	S_2	N_2	K_1	O_1
Avg. amp ATLAS	0.84	0.29	0.17	0.07	0.06
Avg. amp KUTM	0.67	0.32	0.14	0.07	0.06
RMSE amp	0.047	0.014	0.011	0.009	0.007
RMSE vel	0.125	0.043	0.024	0.014	0.012
P amp	99.7	99.8	99.6	97.9	98.4
P vel	85.7	84.9	84.5	76.0	77.4

Table 4.2: RMSE and variance capture (P) of KUTM compared to data listed in Admiralty Tide Tables in the Bohai Sea for tidal amplitude (m), data from paper III

Property	M_2	S_2
Avg. KUTM amp.	0.49	0.13
RMSE amp.	0.05	0.04
P amp.	99.5	95.4

compare the model accuracy in different areas. Readers are directed to the relevant papers associated with this thesis for more information.

4.1.1   Validation of KUTM

KUTM was validated for the European Shelf by Uehara et al. (2006) and it achieved a RMSE of 5-6 cm for the M_2 amplitudes against tide gauge data. However, in paper I further evaluation of the model performance was conducted by comparing the simulated tidal characteristics to those from the OTIS ATLAS (Table 4.1 and paper I).

We also planned to use the OTIS ATLAS to validate the use of KUTM in the Bohai Sea. However, the ATLAS uses a composite of altimetry data from the last 19 years. This has lead to inconsistencies in the solutions for the ATLAS, and there were significant differences between ATLAS and tide gauge data in the north of the domain (Paper III; Fig. 2a). Therefore, for the Bohai Sea we compared the model to the observed values of M$_2$ amplitude and phase listed in Admiralty Tide Tables 4.2.
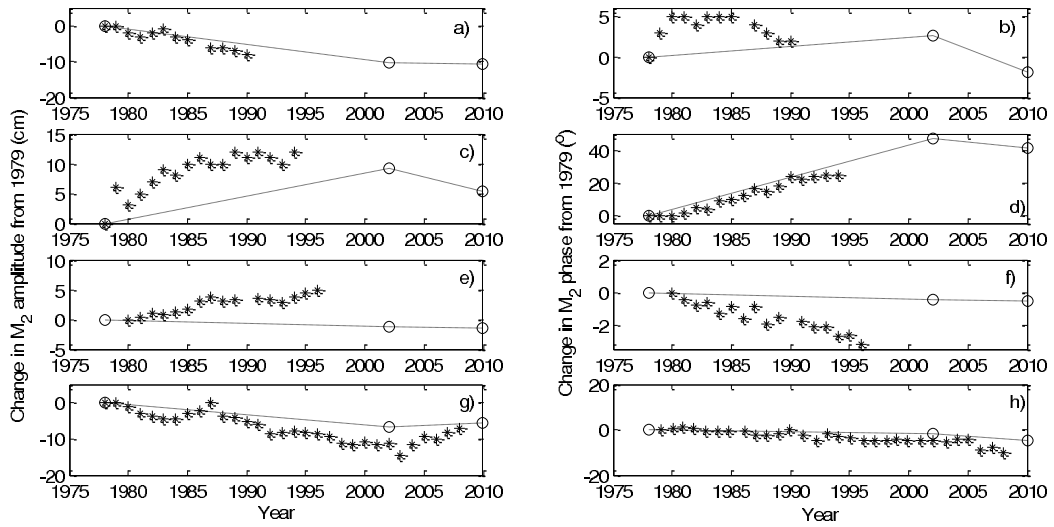
Figure 4.1: 3) Comparison of modelled (black line) and tide gauge (stars) amplitudes (panels a, c, e and g) and phases (panels b, d, f and h) from stations at Longkou (panels a and b), Yangjiaogou (panels c and d), Dalian/Laohutan (panels e and f) and Tianjin (panels g and h).

The rapid land reclamation of the Bohai Sea has opened up a unique opportunity to validate KUTM for long term tidal changes (see Paper III for more information). Unfortunately raw tidal gauge data for the Bohai Sea was very scare, however it was possible to obtain annual amplitudes and phases for M_2 (raw data from a single tidal gauge station (Dalin/Laohutan) and calculated amplitudes and phases from the literature Zhang and Wang (1999); Li et al. (2011)).

With the exception of the phase at Longkou and the phase and amplitude at Dalin/Laohutan the sign of the change of modelled and observed amplitudes and phases are the same (Fig. 4.1). However, the rate of change between the model and observations is not quantitatively consistent suggesting that there are other processes that are important, but the changes in bathymetry are controlling the response (see paper III for further discussion).

KUTM performs well on the European Shelf and the Bohai Sea. Furthermore, we have show that the model shows some skill in recreating the long-term changes in the tidal regime of the Bohai Sea.

Table 4.3: RMSE and variance capture (P) of OTIS compared to tidal gauge data in the Gulf of Maine for tidal amplitude (m), data from paper II.

Property	(M_2)
Avg. OTIS amp.	0.49 m
RMSE amp.	0.069 m
P amp.	99 %

4.1.2   Validation of OTIS

The global version of OTIS (1/12 deg resolution) achieved an RMSE of < 5 cm when compare to TPXO.5 (Egbert et al., 2004). However, we have carried out further validation and compared the tidal characteristics simulated by the model to those from OTIS ATLAS, for each of the regions we have investigated.

In the Gulf of Maine, OTIS compares well with the ATLAS (table 4.3), achieving a RMSE for M_2 of less than 7 cm and a variance capture of 99% (see paper II for details). This is higher than the global value, most probably due to the very large tidal amplitudes characteristic of the region.

OTIS was used in a further study of the European Shelf at higher resolution (Paper IV). The model initially achieved an RMSE of approximately 9 cm. However, due to an inability to resolve coastline complexities, the RMSE was re-calculated on areas deeper that 35m. This gave an RMSE of less than 7 cm for M_2 amplitudes and and a P of 98.7%.

The abundance on long-term tidal gauge data on the EU shelf has enabled us to compare the observed and modelled response of the M_2 tidal amplitudes to observed magnitudes of SLR (Fig. 4.2). This method also allows us to directly compare the response in regions where sea level is falling (e.g. Lerwick) and regions where it is rising (e.g. Newlyn). After the annual sea level and tidal data was extracted the M_2 amplitude was corrected for the 18.6 year cycle (by applying a nodal correction) and sea level was corrected for any vertical land movement (see paper IV for details).

4.2   Inter-model comparison

In order to asses the differences between KUTM and OTIS, and evaluate their advantages. The two models have been set up for the European Shelf at 1/12 x 1/12 degree resolution.
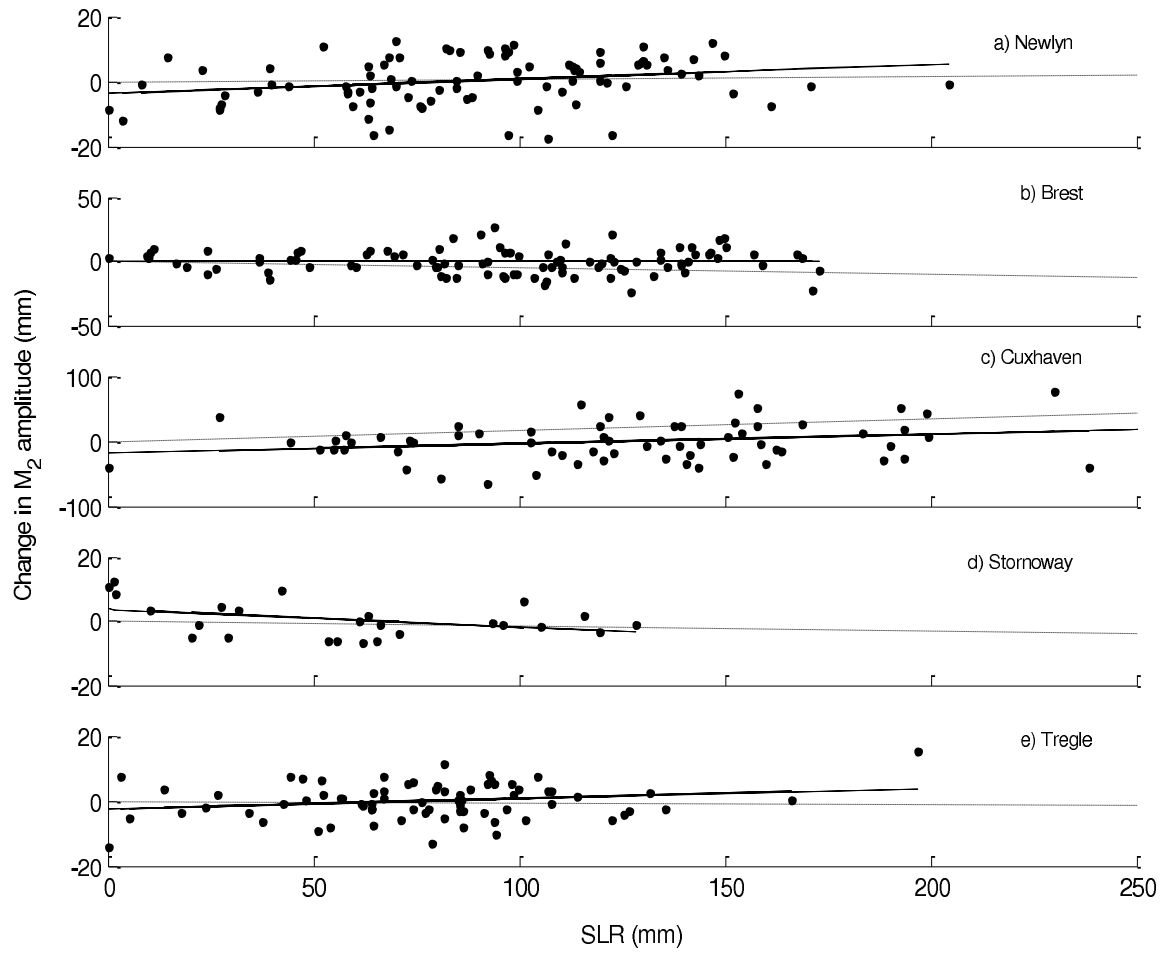
Figure 4.2: Modelled and observed response to SLR from tide gauge station (see paper IV for details). Modelled response is shown as grey dashed lines and annual M$_2$ observations shown as dots. The solid line is the least squares fit from the linear regression of the observations.
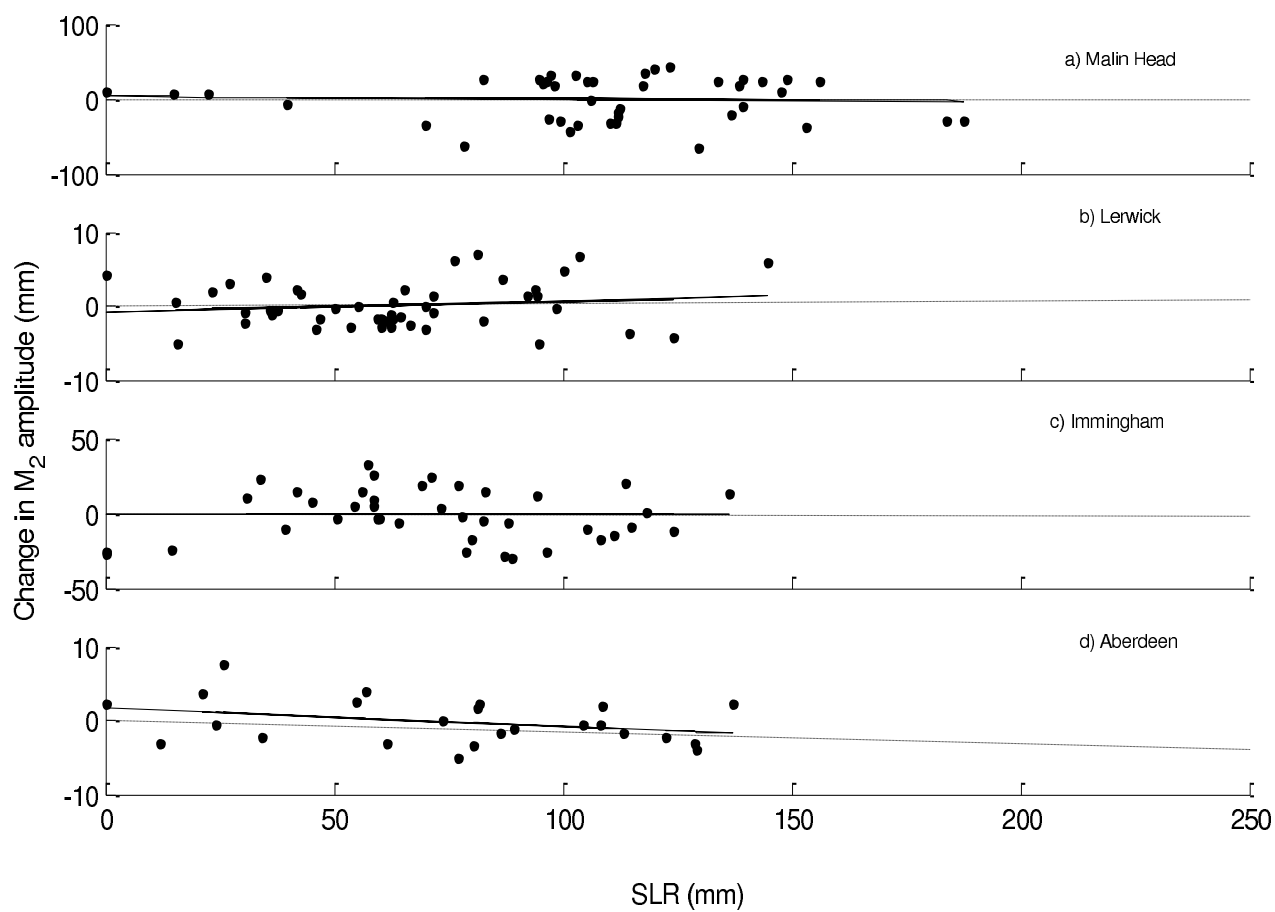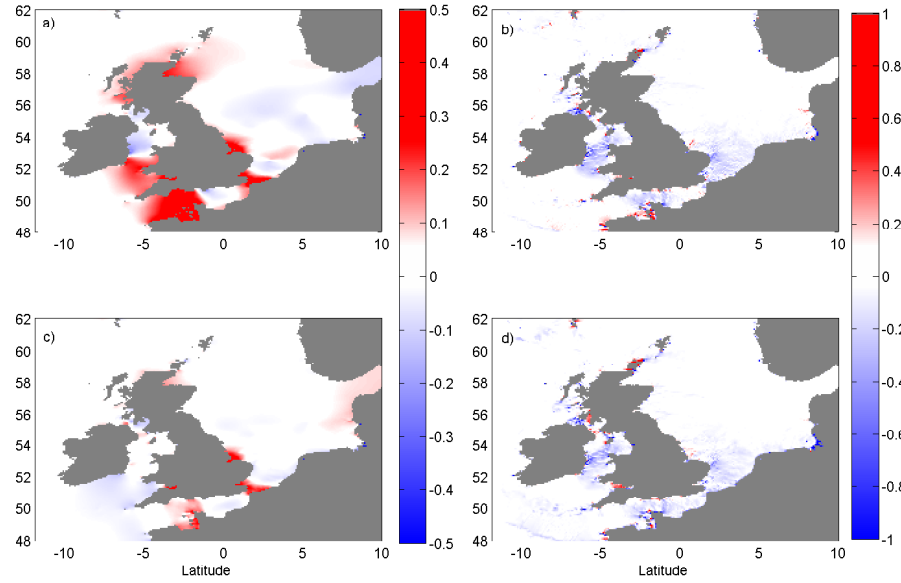
Figure 4.3: As Fig. 4.2

Figure 4.4: The difference between the modelled amplitudes (a and c) and velocities (b and d) compared to the OTIS ATLAS. Results from KUTM are shown in panels a and b, and results from OTIS are shown in panels c and d.

Both simulations have used the KUTM bathymetry grid (as described in Uehara et al., 2006) and the same set up as described in paper I. In the following only the M_2 constituent will be dealt with, as it is the dominant constituent.

Fig 4.4 shows the difference between each model's tidal amplitudes and velocities and the equivalent solutions from the OTIS ALTAS. There are some significant differences between the solutions the models have calculated, mainly in the tidal elevation. OTIS appears to overestimate the M_2 amplitude over much of the shallow shelf with the exception of a small area in the Irish Sea. KUTM compares better to the ATLAS, but still overestimates some shelf areas. Both models underestimate the tidal velocities on the shelf.

The is also a difference in the RMSE calculated for each model. While KUTM achieves a RMSE of 0.047 m for M_2 tidal amplitudes, OTIS only achieves 0.095 m. Furthermore KUTM achieves a variance capture of 99.7 % while OTIS only achieves 98.7 %. The RMSE both models achieve for tidal velocity is higher than the amplitudes (0.12 m and 0.125 m

for OTIS and KUTM respectively). The variance capture is also lower (86.7 % and 85.7% for OTIS and KUTM respectively). It should be noted that the set-up employed has been tuned with KUTM, so a better fit to the ATLAS is likely to be achievable with OTIS after appropriate tuning.

There are a number of reasons that the models may differ. Although there are not significant differences in the boundary conditions used by each model, the way they are implemented does differ significantly. OTIS is only forced by elevations whereas KUTM uses both elevations and velocities, this would suggest that in this instance forcing by tidal velocities improves the accuracy of the simulation. Furthermore, as the Baltic Sea is enclosed, OTIS assumes it is a lake and masks it off (i.e. will not take boundary conditions from that region).

4.2.1 SLR implementation

A comparison has been made between the response of the two models to 5 m SLR. The SLR has been implemented using the flood and no flood methodology described in section 3.1.3 and both models used the set up described in the previous section. Each simulation of M_2 amplitude from the SLR runs has been compared to the present day (control) run for it's respective model, thus the impact of the differences between the models already discussed in the previous section should be kept to a minimum.

Figure 4.5 shows that both models suggest similar the impacts of 5 m SLR on the M_2, including how SLR is implemented. The only difference is in the Kattegate where OTIS suggests an increase in the flood run and KUTM does not. It is possible that this is connected with the way in which both models deal with the boundary conditions in the vicinity of the Danish Straits.

4.3 Sensitivity simulations

In order to fully assess the tidal model capacity and to ensure all the important processes are simulated a number of sensitivity tests were run for the European Shelf. Most of the runs were completed with both KUTM and OTIS (set up using the same parameters as Paper I, described in section 3.4). However, for the sake of computational speed OTIS only was used for the higher resolution runs. A model-model comparison of the control runs can be found in section 4.2, which should be kept in mind when evaluating these
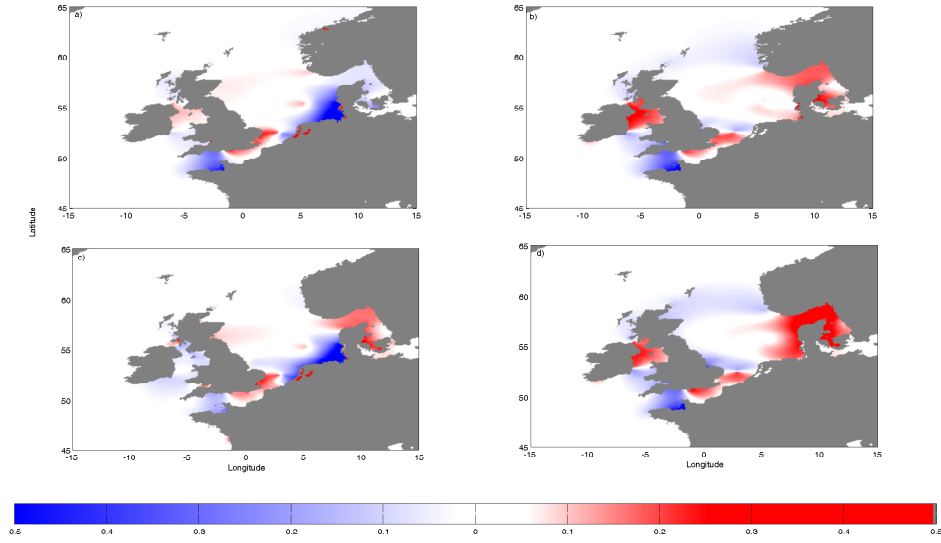
Figure 4.5: The response of the M_2 amplitude (m) simulated by KUTM (a and b) and OTIS (c and d) to 5m SLR, using the flood (a and c) and no flood implementation (b and d) methods.

simulations. However the difference plots will not compare the different models (i.e. the difference is the perturbation minus the control of each model). Testing the effectiveness of these additional processes is conducted by calculating the RMSE compared to OTIS ATLAS for each new simulation (as OTIS ATLAS also contains tidal gauge data in its assimilation). In this study we have concentrated on the M_2 tide only as this is the dominating constituent on the European Shelf.

4.3.1 Bed friction coefficient

It is common practice to adjust bed friction in order to improve model accuracy (i.e. the bed friction coefficient is a tuneable parameter). The impact of changing the bottom friction coefficient is concentrated in the shallow waters where the influence of bed friction is at its strongest. Increasing the bed friction decreases the tidal amplitude as more energy is removed as dissipation, conversely decreasing the bed friction coefficient increases the tidal amplitude as less tidal energy is lost.

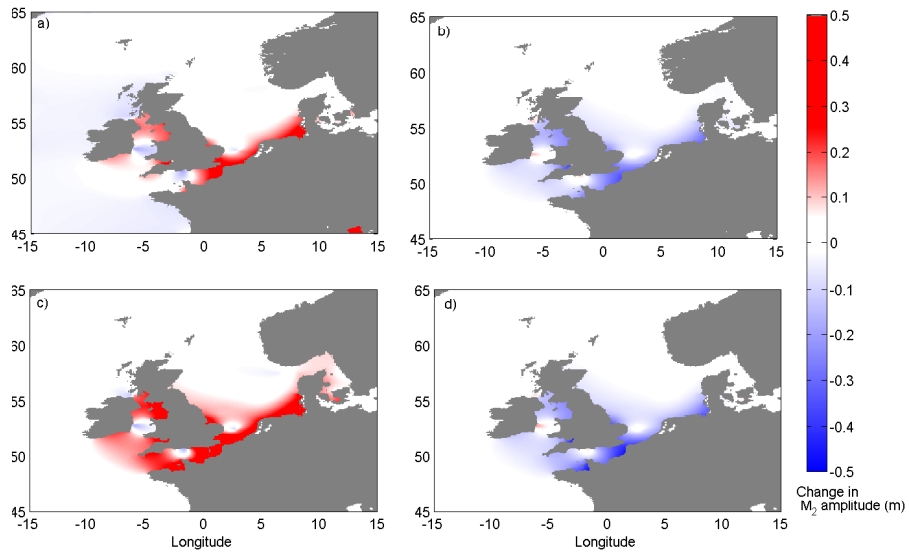Both models react in a similar fashion, with the same magnitude of sensitivity to

Figure 4.6: Impact on the M$_2$ amplitude of changing the value of bottom friction coefficient (control $C_d = 2.6 \times 10^{-3}$) using KUTM (a and b) and OTIS (c and d). Panels a and c show the effect decreasing C_d to 1.6×10^{-3}. Panels b and d show the effect of increasing C_d to 3.6×10^{-3}.
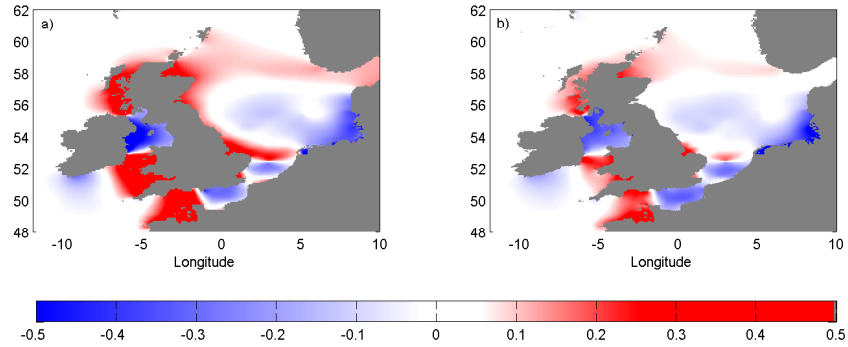
Figure 4.7: Difference in M$_2$ amplitudes compared to the OTIS ATLAS, with a grid resolution of $1/12^o$ in both longitude and latitude (a) and $1/60^o$ in both latitude and longitude (b).

changes in the bottom friction coefficient.

4.3.2   Grid resolution

Higher resolution runs were conducted at a resolution of $1/60^o$ in both latitude and longitude for the European Shelf using OTIS with the GEBCO bathymetery database. These were compared to runs also using OTIS and GEBCO, but at a resolution of $1/12^o$ in both longitude and latitude. Increasing the grid resolution decreased the RMSE from 0.16 m to 0.11 m. Figure 4.7 shows the simulated M$_2$ amplitude compared to the OTIS ATLAS.

4.3.3   Bathymetric databases

We also test two high resolution global bathymetric databases (GEBCO Ward (2010) and Smith and Sandwell, hereafter S&S, Smith and Sandwell (1997)). The databases have been averaged to a resolution of $1/12$ of a degree. There are significant differences between these bathymetries and the control bathymetry (Uehara et al., 2006, Paper I).

Neither simulation using either model or either global database accurately reproduces the tides on the European Shelf. The GEBCO simulation gave an RMSE = 0.09 m and the S&S simulation had an RMSE = 0.14 m using KUTM and 0.16 m and 0.12 m using OTIS. There are significant differences (when compared to the soundings based bathymetry used in the control, see Fig. 4.11) between both the databases tested. GEBCO underestimates the water depth throughout much of the North Sea and the Irish Sea by and average of 16 cm, whereas S&S underestimates most of the west side of the North sea with the exception of several large banks.

4.3.4   Bed roughness

Random values in a range of ±2m, ±4m and ±8m were added to the shallow water areas (H<200m) part of the control bathymetry in order to asses the effect of bathymetry has on the response of the (M_2) amplitude. As seen in Fig. 4.9 the model is sensitive to the magnification of the random bathymetry added, ±2m gives little difference from control, where as ±8m shows a very significant change. The effect of random bathymetry intensifies towards the Danish Straits due to the propagation of the tide through the North Sea. The results from the different models do differ, the OTIS simulations suggest far less sensitivity to bed roughness.

4.3.5   Wetting and drying

During this project KUTM was modified with the addition of a wetting and drying (WAD) scheme based on Oley (2005). The scheme identified the intertidal zone and can assigned the relevant grid cells as either wet or dry. In order to solve the equations of motion for the dry cells, they are given a very shallow (in the order of cm) finite water depth and velocities are set to zero if the water depth falls to this level. The effect of running KUTM and OTIS with WAD had a substantial impacts on the tidal regime throughout the domain. However, because of the coarse resolution of the model, which overestimated the intertidal area WAD significantly decreased the accuracy of both models.

   However, when the wetting and drying was implemented in the higher resolution, the impact was smaller and we would suggest more realistic as the inter-tidal zone was more accurately represented (reduced the RMSE from 0.099 m to 0.097 m).
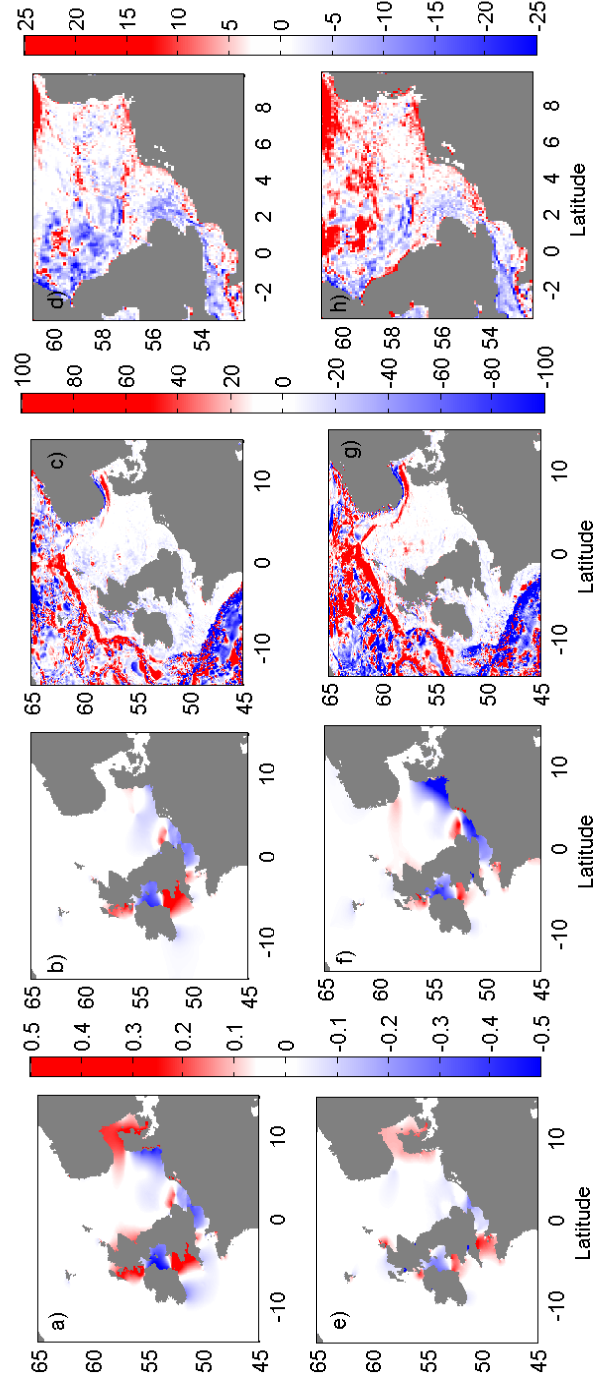
Figure 4.8: The impact on the M_2 tidal amplitude (a,b,e and f; units are m) of different bathymetry databases: GEBCO (a) and Smith & Sandwell (e). Also shown is the difference in the water depth (m) between these two databases and the control bathymetry (c and d for GEBCO and g and h for Smith & Sandwell). Panels a and e are the results from OTIS and b and f are results from KUTM.
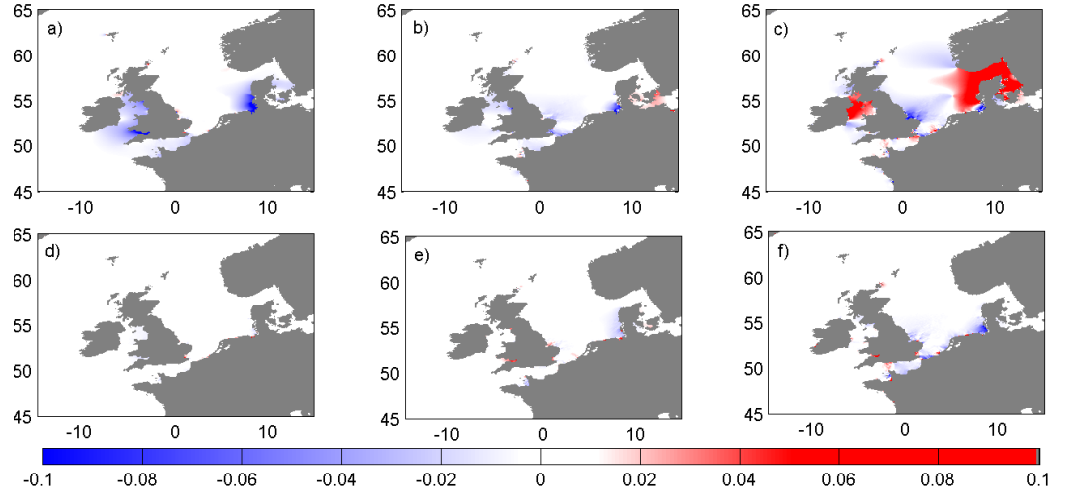
[t]

Figure 4.9: Impact on the M_2 amplitude of adding random values in the range of ± 2m (a and d), ± 4m (b and e) and ± 8m (c and f) to the shallow water areas (H<200m) in the control bathymetry. Results from KUTM are shown in panels a-c and for OTIS in d-f.

4.3.6   Tidal energy conversion and tidal potential

Within this project a tidal conversion parametrizations was also implemented within KUTM based on Zaron and Egbert (2006). The parametrisation of tidal conversion showed significant tidal energy dissipation due to internal wave generation. However, this had very little impact on the tidal amplitudes. Runs were also conducted with no tidal potential acting on the domain. These runs also showed very little difference from the control runs.

4.3.7   Boundary forcing

Like the bed friction coefficient, it could be argued it is standard practise to tune the boundary conditions in order to get a higher model accuracy (see Young et al., 2000). We have conducted fours runs for both models, increasing the tidal amplitude and velocity by 5% and 10%. In the KUTM simulations the main impacts are mainly restricted to the shallow water coastal areas and to the south western regions of the domain. This is simply because the western boundary is a large open ocean boundary with reasonably large tidal amplitudes and velocities (for open ocean tides). The OTIS simulations show a slightly different impact (Fig. 4.3.7). Although the response is still mostly linear, it is not as large

as response shown by KUTM. This suggests that KUTM is more sensitive to boundary forcing compared to OTIS.

It is possible that the boundary conditions could subdue any tidal response to an on-shelf perturbation (Garrett and Greenberg, 1977). For example, in paper II boundary conditions were kept constant with increasing SLR. As SLR is expected to increase globally, we investigated if changes in the global (open) ocean affect our boundary conditions and if these changes in boundary conditions affect the response of the tides to SLR on the European Shelf. The effect of the new boundary conditions on the response of the tides to SLR is insignificant (<1 cm).

4.3.8   Summary

The validity of any model results depends on the accuracy of the model employed. Thus validating the tidal model used for each scenario is crucial for the confidence of any further studies. For each scenario in this thesis we have shown that compared to either OTIS ATLAS or tidal gauge observations the models perform at least acceptable (i.e. the error associated with the model is significantly less than the signal under investigation).

It is also important to asses the sensitivity of the model to different processes and set-ups, as it is important all relevant processes are included and conversely for the sake of computational power all unnecessary processes are not included. The results shown here show that the tidal models are very sensitive to bathymetry and thus it is vitally important the most accurate bathymetry is used. Furthermore the model is sensitive to varying boundary conditions although important for this thesis the response of the tidal system to SLR is not significantly changed with varying boundary conditions. Wetting and drying has shown to have a small impact of the tidal system, but useful results depend on how accurately the intertidal areas are represented. At low resolution the intertidal areas are not resolved fully and adding the process of wetting and drying significantly decreases the accuracy of the model. Other processes such as tidal energy conversion, while important in specific areas (e.g. Green and Nycander, 2013), do not have a significant impact on the tides in these simulations. The grid resolution is often dependant on the resolution of the bathymetry and computational power available, thus a balance has to be met and these simulations would suggest that the accuracy of the bathymetry is more important than grid resolution.
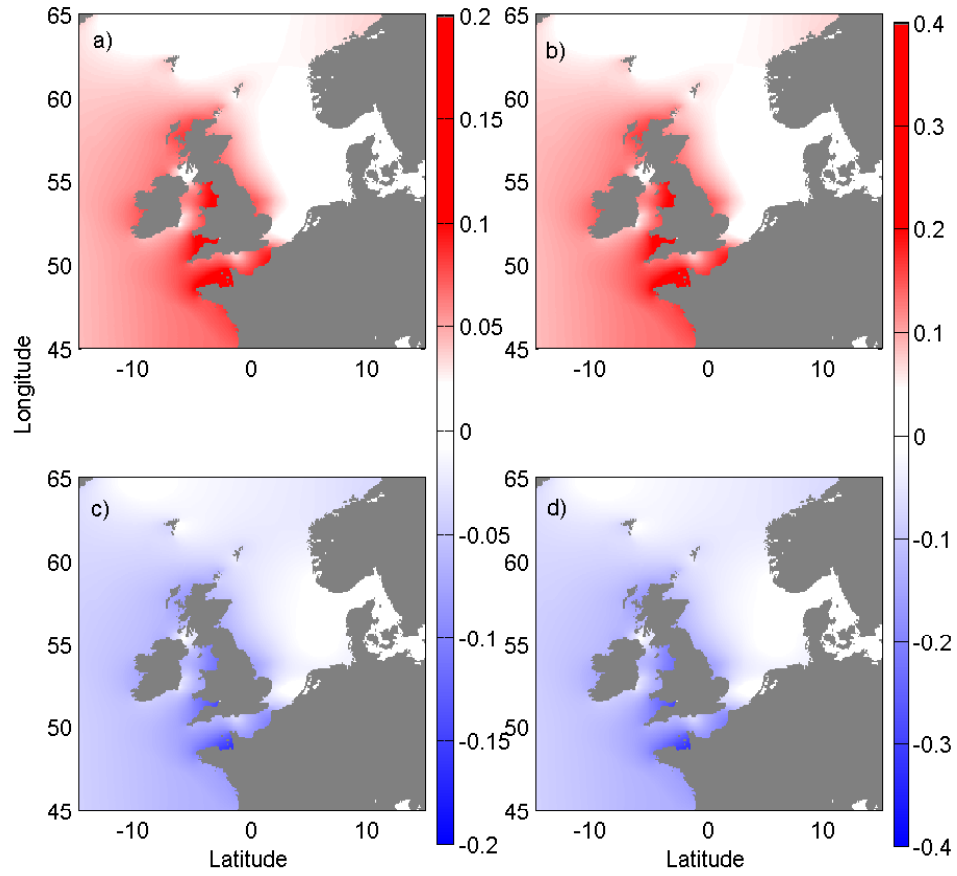
Figure 4.10: The impact on the M_2 tidal amplitude of increasing (a and c) and decreasing (b and d) the boundary conditions by 5% (a and b) and 10% (c and d) using the KUTM model.
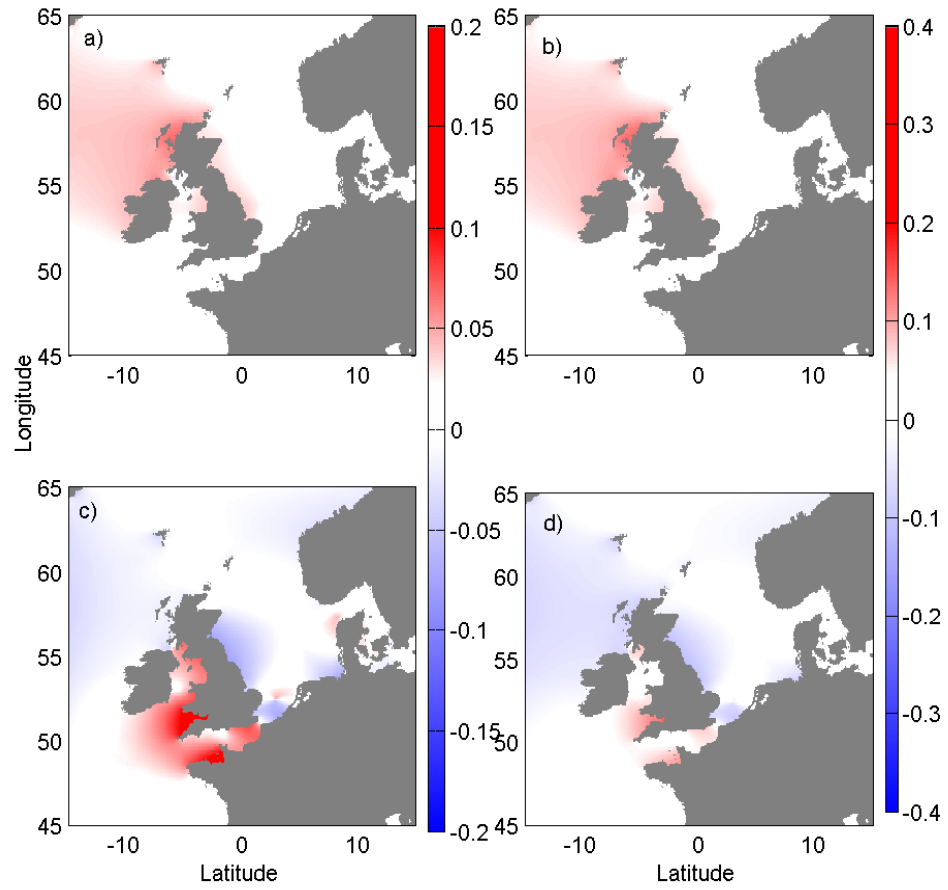
Figure 4.11: The impact on the M_2 tidal amplitude of increasing (a and c) and decreasing (b and d) the boundary conditions by 5% (a and b) and 10% (c and d) using the OTIS model.

Part II

Part II: Summary

5 Investigating Seas of the Future

The IPPC has said that current sea level is rising and that the rate of SLR may increase in the future (Nicholls et al., 2011a). Furthermore, growing populations have increased the need for land reclamation and clean energy in the form of tidal power plants. How these projected changes could impact the tides is of significant importance to coastal communities.

5.1   Sea level rise

Three components make up high water levels; surges, tides and the water level (datum) itself. Surges are caused by set-up from the wind blowing water into the land and occurs over relatively short time scales, making them difficult to predict. On the other hand sea level changes very slowly, but as the forcing for these changes is not fully understood it is also difficult to predict. As tides are forced by the gravitational pull of primarily the moon, the forcing is essentially constant (over decal to centennial time scales) and therefore highly predictable. However, while the tidal forcing does not change, the effect of the tides - such as tidal phase and amplitude is highly dependent on bathymetry and energy dissipation and therefore can change over time.

Direct observations of sea level have only been available over the past century (other than a couple of notable exceptions e.g. Stockholm, Sweden), through the use of tide gauge data (see also section 3.3). While the long term tide gauge database is somewhat patchy in terms of spacial and temporal resolution, some estimates of the rate of SLR have been made (e.g. Church and White, 2006; Holgate, 2007). Furthermore, over the past two decades satellite altimetry has enabled accurate, high temporal and spatial resolution global sea level data (e.g. Egbert et al., 1994; Egbert and Ray, 2001; Leuliette et al., 2004), reducing
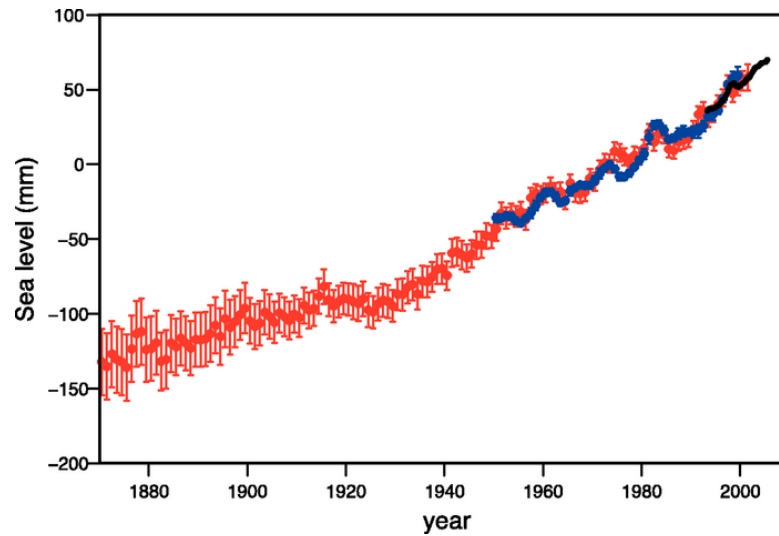
Figure 5.1: Annual averages of global sea level (mm). Red and blue dots are derived from tidal gauge data and black is from satellite data. Observations are deviations from the average of the period 1993–2001 (in red) and 1961–1990 (in blue and black). Error bars show the 90% confidence interval (IPCC and references within)

the error associated with previous estimates and highlighting regional differences in the rate of sea level change (Denman et al., 2007). Figure 5.1 shows various estimates of global sea level and the error associated, it highlights the reducing error as sea level observations become more accurate.

Making projections of expected rates of future sea level change is inherently difficult, especially when the drivers of sea level changes are not well known (see following section) and thus there is significant variation between projections. The IPCC reports a projected sea level rise of 0.18 - 0.59 m by 2099 (Nicholls et al., 2011a), however it has been suggested that these projections may be exceeded (see Nicholls et al., 2011b, for a review). Whilst the IPCC suggests that the ice sheets will discharge linearly, recent studies have suggested this is not the case and the rate of sea level rise may be higher (Rahmstorf, 2007; Rohling et al., 2008; Pfeffer et al., 2008; Kopp et al., 2009; Vemeer and Rahmstof, 2009; Grinsted et al., 2009).

Figure 5.2 shows a number of approaches recently used to make future projections of sea level rise. Both Rohling et al. (2008) and Kopp et al. (2009) have used a paleo-oceanographic approach. By analysing SLR rates from the last interglacial stage, which
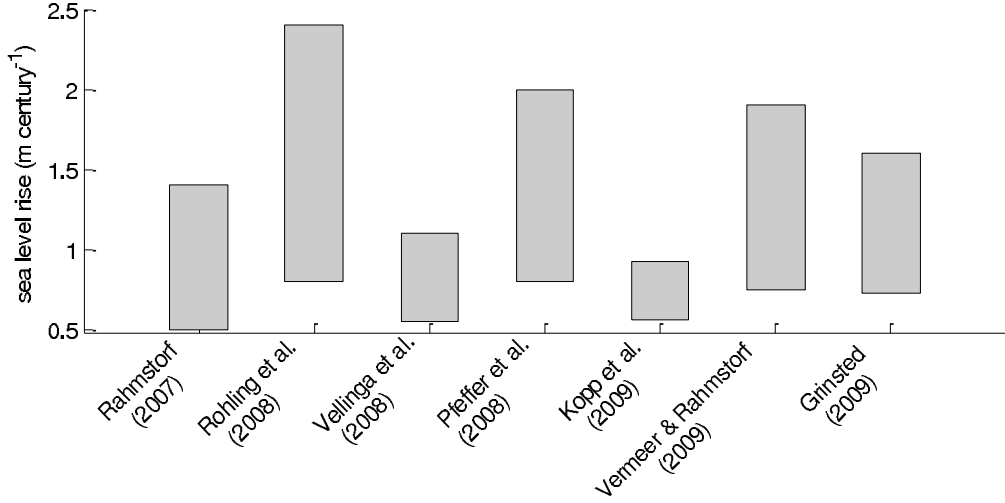
Figure 5.2: Number of recent estimates of present day rates of SLR. The methodologies used are discussed in the text.

exhibits similar temperatures and ice sheet masses to present day, Rohling et al. (2008) and Kopp et al. (2009) were able to make estimates of present day rates of SLR and the differences between the two studies lie in the proxies they have used to obtain the paleo-SLR rates. As their estimates barely overlap, this is a suggestion of inaccuracy with the proxies employed. While Pfeffer et al. (2008) did not make SLR rate predictions, they do provide an estimate of the upper limit of global SLR, by exploring the potential of glacial melt water to provide more than 2 m SLR. Semi-empirical methods have been used by Rahmstorf (2007), Vemeer and Rahmstof (2009) and Grinsted et al. (2009) to predict future SLR rates for the IPCC AR4 scenario. This involved using temperature results from climate-model projections and present day relationships between temperature and sea level. The differences between the projections is mostly down to small differences in statical methods (Nicholls et al., 2011b).

The rate of relative sea level change (ΔRSL) is a sum of several components that occur a various temporal and spatial scales and can be described by the following equation (Nicholls et al., 2011a):

$$\Delta RSL = \Delta SL_g + \Delta SL_{RM} + \Delta SL_{RG} + \Delta SL_{VLM} \tag{5.1}$$

where ΔSL_g is the variation of global sea level, ΔSL_{RM} is the variation due to meteo-
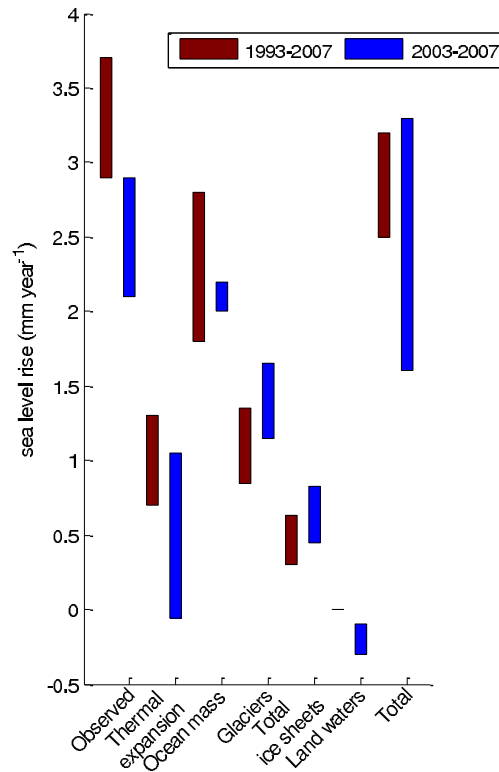
Figure 5.3: Number of recent estimates of the components of present day rates of SLR (based on data from Cazenave and Llovel, 2010)

oceanographic processes, ΔSL_{RG} is the variation due to changes in the Earth's gravitational field and ΔSL_{VLM} is the variation due to vertical land movement. Recent estimates of the contributions to present day SLR rates are shown in Fig. 5.3.

Global mean sea level change refers to two main processes. The first is eustatic changes, these are where water mass is added or removed from the ocean. This can be due to the melting of glaciers and icecaps or/and changes in the mass balance of the Greenland and Antarctic ice sheets. The second process are steric changes which include changes to sea level due to thermal expansion.

Cazenave and Llovel (2010) have continued the approach of the IPCC AR4 and produced estimates of the individual components contribution to sea level change (Fig. 5.3.). They show that during the period 1993-2007 the estimated rate of SLR underestimated the observed rate of SLR by 0.45 mm year^{-1}. However, during the period 2003-2007 the estimates are far closer to the observations (a difference of 0.05 mm year^{-1}).

Surprisingly, even the moderate SLR the ocean has experienced over the last few decades (a fraction of a meter) has already had an impact on global (e.g Woodworth et al., 2009; Muller et al., 2011) and regional tidal systems (e.g Flick et al., 2003; Ray, 2009; Jay, 2009). Modelling studies have also shown that globally there are tidal impacts of SLR (Egbert et al., 2004; Green, 2010; Muller et al., 2011), but these changes are poorly captured by global tidal models due to the low resolution of the models. Furthermore, the models themselves differ significantly in the magnitude of these changes; from a relatively coarse global simulation, Green (2010) suggests that even with 5 m SLR there are only minor impacts on the global tidal dissipation but significant impacts on tidal amplitudes, and Muller et al. (2011) suggested that there have been significant global changes in the tides related to SLR over the last century, although it is possible that this may be because of the way SLR is implemented.

Three recent studies of tides and SLR on the European Shelf show very different local responses in some areas (Roos et al., 2011; Pickering et al., 2012; Ward et al., 2012). Paper I shows, that flooding of land significantly alters the response of the tides to SLR on the European Shelf, in contrast to simulations where vertical walls were introduced at the present day coastline before the SLR was implemented. Newly flooded areas will have high tidal velocities due to their shallow water depth, and consequently dissipate significant amounts of tidal energy due to bed friction. This effect shifts the amphidromic points towards the locations with enhanced dissipation (Taylor, 1921) and significantly alters the tidal regime. On the other hand, the introduction of high vertical walls at the present day coastline, which prevents the flooding of new cells, introduces changes in the propagation speed of the tidal wave, but may also impact on the resonant properties of the certain basins (e.g Arbic and Garrett, 2010; Green, 2010, Paper I). The response of tidal systems to SLR can be highly non linear due to additional shallow water effects, such as resonance. Paper II shows that the tides of the Bay of Fundy may increase with SLR as the increasing water depth brings the natural resonance period of the basin closer to the M_2 frequency. However this only occurs when there is no flooding and it is suggested in Paper II that when flooding is allowed to occur the change in dissipation is enough to alter the resonant properties of the basin (see also Greenberg et al., 2012).

The contrasting response of the regional tidal systems to the implementation methods of SLR opens for an interesting research question, how do flood defence schemes effects the response of the tides to SLR? Paper III shows the affect of SLR on the tidal system of the

Bohai Sea, China. SLR was implemented in three ways; flooding, no flooding and a partial flood where flood defences were added as vertical walls along sections of the coastline. In this scenario the response of the partial flood runs was very similar to the flood runs. However, in Paper IV the partial flood runs showed additional impacts on the European Shelf to the flood and no flood runs with small (<1 m) SLR. Flood defences (based on Govarets and Lauwerts, 2009) allow some areas to flood and flood waters to build up behind the flood defences themselves. This causes the formation of narrow channels which will funnel the tides causing high velocities and change the geographical distribution of tidal energy dissipation in areas of high tidal range (the Severn Estuary and the English Channel). However, it does not appear that this process occurs when the Netherlands flood, it is suggested that this is because the large newly flooded area will be very shallow and as the present day tidal range is small in that area the time in which the area will actually be underwater is small.

5.2 Tidal power plants

5.2.1 Introduction and theory

The global tides potentially represent a reliable, predictable and clean energy resource. The intermittent nature of other renewable resources such as wind and solar energy make power supply from them unreliable. The motions of the tide are well known, and thus very predictable.

The extraction of tidal energy involves the transformation of kinetic energy within the moving fluid into electrical energy, though the use of a generator. The simplest method of extraction is termed free-stream, where a turbine is situated within the water column and the flow around it forces the turbine to turn a generator. This method is analogous to a wind turbine, with the advantage of a denser medium and more predictable currents. The starting place for early potential tidal energy extraction predictions is a calculation of the kinetic energy flux of flow through a channel, given by:

$$P = \frac{1}{2}\rho A \overline{u}^3 \tag{5.2}$$

where ρ is the density of seawater, A is the cross-sectional area of the channel and $\overline{u}$ is the mean flow velocity across A.

However, this method does not consider the fictional or turbulent effects of the flow nor the nature of the free-surface between the seawater and the atmosphere. This method met further criticism when Garrett and Cummins (2005) found that although the kinetic energy flux suggests the presence of extractable energy, it bears no simple relation to the power output. They proposed a relationship where:

$$P_{max} = \gamma \rho g a Q_{max} \tag{5.3}$$

Where ρ is the density of seawater, a is the amplitude difference between the channel ends, Q_{max} is the maximum volume flux in the natural tidal regime and γ is a coefficient that depends on whether the estuary is forced by friction or acceleration (Garrett and Cummins, 2005). This relationship suggests that the geographical nature of the site as well as the kinetic energy flux is important. Tidal free stream tidal turbines introduce an additional drag term on the flow (Bryden and Couch, 2006), therefore it is possible to parametrize the turbine as an additional term (K_t) in the quadratic bottom friction formulation (see Eq. 3.6):

$$\mathbf{F} = (C_d + K_t)\mathbf{U}|\mathbf{u}|/H \tag{5.4}$$

The power associated with K_t, i.e. from the turbine only, can be estimated following Garrett and Cummins (2005); Sutherland et al. (2007); Blanchfield et al. (2008); Karsten et al. (2008):

$$P_t = P\frac{K_t}{K_t + C_d} \tag{5.5}$$

where:

$$P = \rho(C_d + K_t)\overline{(u^2 + v^2)}^{3/2}A \tag{5.6}$$

Here ρ is the density of sea water and A is the horizontal area in which the energy is to be extracted. As K_t increases so does P until, in geophysical flows, a limit is reached after which P will decrease with increasing K_t. This is because if too many turbines are placed in a channel the drag they create would slow the current, and thus reduce the maximum power output of the power station. Therefore there is a theoretical maximum to the amount of power available in a realistic application (Bryden et al., 2004; Garrett and Cummins, 2005).
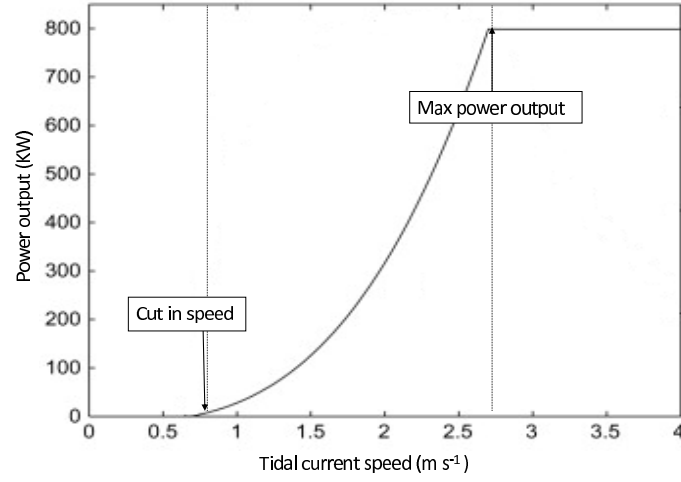
Figure 5.4: Generic power output curve of a current turbine as a function of current velocity. Highlighted is the cut in and maximum power output

This is a popular approach to estimate the maximum extractable power from a free-stream tidal power station and has been used for the Bay of Fundy (Karsten et al., 2008; Hasegawa et al., 2011, and paper II), the UK coastal waters (Walkington and Burrows, 2009) and many other situations (e.g. Sutherland et al., 2007; Blanchfield et al., 2008).

With the advent of the production of tidal power turbines more realistic predictions of extractable power have been produced, based on the specifications of the turbines themselves. At very low current speed the kinetic energy available will not be sufficient to turn the turbine thus no energy will be produced. The lowest level of current speed needed is known as the cut-in speed (typically under 1 m s^{-1}). Conversely there is also a maximum current speed that the turbine will produce power (Fig. 5.4).

Neill et al. (2009) used a realistic power curve from a Seagen marine current turbine which allow a parametrization whereby the shear stress evolves over the tidal cycle. The parametrization also has a realist cut-in and rateable power output;

$$\tau = \frac{P_x}{\rho u \delta x B(h + \eta)} \tag{5.7}$$

where P_x is the power extraction, ρ is the density of seawater, δx is the model grid spacing, u is the current velocity, h is the mean water depth and η is the variation of

the free surface from the mean water level. As in this project we were not able to obtain realistic power output curves from the turbines planned we could not used this approach. instead we have estimated the maximum power output.

5.2.2   Impacts of free stream tidal power plants

As free stream tidal power plants remove some of the tidal energy it is likely that there will be some impact on the tidal dynamics of a system. As there have not been many TPPs that remain functional for a substantial period of time it is difficult to accuracy assess any impacts. La Rance, France (a tidal barrage) is the only area in which any ecological impacts, or the ability of the ecosystem to recover, can be physically observed. A study by Retiere (1994) showed that the tidal barrage has not had a detrimental effect on the recolonization of the estuary basin, suggesting that the tidal barrage is permeable for most species typical of the area. The study shows that 10 years after the installation the ecology of the region was able to reach a new ecological equilibrium, with a loss of biodiversity to the previous regime. Further studies (e.g. Kirby and Retiï¿½re, 2009) have suggested that the ecological effects on a Severn barrage scheme would be similar to the effects seen at La Rance, although a further study by Pethick et al. (2009) points out that using the La Rance as a model for estuarine change is 'unhelpful' and argues that any changes are highly specific to the estuary in question.

A study by Neill et al. (2009) showed that the presence of tidal stream turbines could have a significant effect on the large-scale morphodynamics, although this is highly dependant on the tidal asymmetry at the point of energy extraction. Over the life cycle of the turbine (30 years) it was predicted that the bed-level could vary by up to 4m. Modelling studies have shown that there are significant far-afield effects of a combination of tidal power plants in the Severn, and Eastern Irish Sea (Wolf et al., 2009; Ward et al., 2012). Furthermore, these effects increase when combined with sea level rise (Ward et al., 2012).

The large tidal range of the Gulf of Maine has attracted the attention of renewable energy industries, keen on exploiting this natural resource. However, the tides in the Gulf are extremely sensitive to the implementation of TPP due to feedbacks induced by the increased dissipation of tidal energy (Garrett and Cummins, 2005; Sutherland et al., 2007). For example, (Karsten et al., 2008, Paper II) has shown that the placement of free stream TPP in Minas Passage could affect the tides as far away as the Bay of Boston. However studies have shown that removing energy from only the bottom half of the water
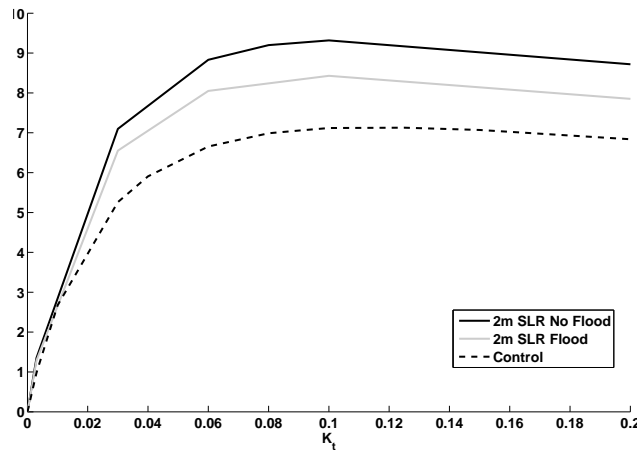
Figure 5.5: Maximum power output (GW) for a free stream TPP in Minas Passage as a function of turbine friction, K_t. The control results are shown in solid black, whereas grey and dashed lines show the response with 2 m SLR for the flooding and no flooding cases, respectively.

column may reduce the impacts (Hasegawa et al., 2011). Paper II showed that the effects of SLR and free a stream tidal power plant can simply be added (i.e. there is not effects of the processes interacting with each other), but that the effects of the tidal power plants significantly out-weighed those of SLR. Furthermore paper II shows that the maximum power output of the Minas Passage in the Bay of Fundy increases with future SLR (Fig 5.5).

5.3   Land reclamation

The average population density of coastal areas is almost twice the global average (Creel, 2003). Growing populations and over crowding of developed areas has lead to the need to reclaim land from the sea. The idea of land reclamation is not new; evidence of Neolithic Chinese paddy fields and ancient fish ponds show land was reclaimed by enclosing a coastal or estuarine area. However, in the present day land reclamation is mostly used as a method of dealing with landfill sites and increasing the land area in highly developed areas. Global estimates of land reclamation are scarce, however there are a number of countries that have reclaimed significant amounts of land from the sea (e.g. Glaser et al.,

1991; Hoeksema, 2007, see also Fig 1.1). Quantifying the hydrodynamic and ecological impacts of land reclamation can be difficult (Ni et al., 2002). Almost 1/6 of the total area of the Netherlands is land reclaimed from the sea (Hoeksema, 2007, and Fig. 5.6) and there is the suggestion that this could have significantly changed the tidal and wave dynamics of the region (Schouten, 2006).

Other areas of significant land reclamation include Hong Kong, where 9.38 km^2 of land was reclaimed from Victoria Bay to construct an airport (Pickles and Tosen, 1998). Significant impacts on the tidal regime from land reclamation, including sediment transport has been detected in the area (So, 1986). Land reclamation in the Bohai Sea has been rapid and extensive over the past 35 years (Fig. 5.7), which have been caused by both natural and anthropogenic factors (Paper III). The shift of the river mouth of the Yellow River commenced in 1976 and has created a spit-like feature extending as far as 20 km in the western coast of Laizhou Bay. Furthermore, human activities along the western coast have resulted in the formation of reclaimed lands as large as 700km^2, comparable to the land area of Singapore, in the last decade. Significant changes in the tidal regime have been observed in the same region over the past three decades (Zhang and Wang, 1999; Li et al., 2011). Paper III shows that the changes in the coastline have had a significant impact on the tidal regime of the region. Furthermore, the changes in the coastline have made the Bohai Sea, in some places, more susceptible to the tidal impacts of SLR.

Figure 5.6: Areas of the Dutch coast reclaimed. Figure from: http://www.planetware.com/map/netherlands-land-reclamation-on-the-north-sea-coast-map-nl-nl2.htm
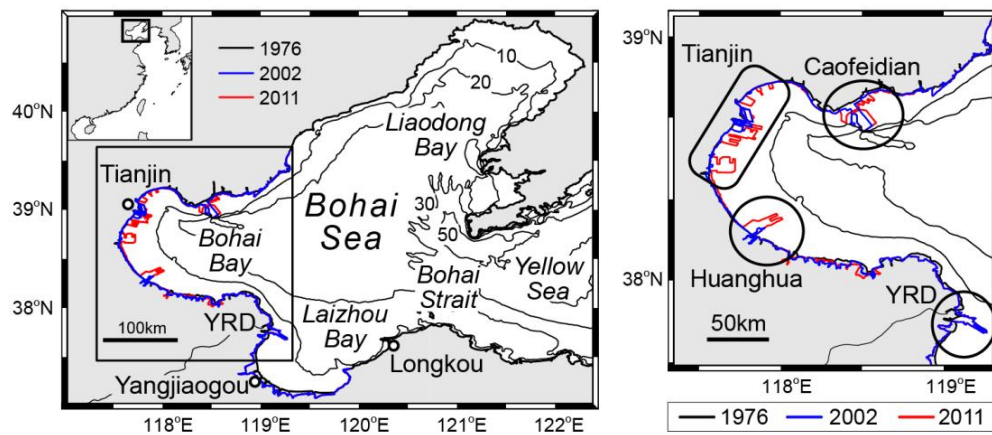
Figure 5.7: 1976 bathymetry of the Bohai Sea and a close-up view of Bohai Bay. Coastlines from the 2002 (blue) and 2011 (red) bathymetry are plotted on top.

6 Conclusions and Recommendations for Future Work

Using regional numerical model simulations we have been able to quantify the sensitivity of the tides in these regional set-ups to sea level rise, free stream tidal power plants and land reclamation. Each of these scenarios results in variation in the tidal energy dissipation field and in some instances impact significantly on the regional tidal regimes.

The models and set-up employed with papers I and II are simple, with the aim of identifying the controlling mechanisms as opposed to make predictions. Whereas papers III and IV use a somewhat more complex and realistic set-up to make predictions underpinned by validation using long term tide observations. The models used for each study have been validated for the present day tidal systems and perform reasonably well. Furthermore we have been able to use long-term tide gauge data to compare the trends of observed and modelled tidal properties to add further confidence in our results.

Primarily flood defence schemes have localized benefits (i.e. to defend the coastline they protect), however we have shown that the process of flooding or not can have basin wide tidal impacts. Which when combined with storm surges could contribute to further flooding. Thus the impact of changing tidal regimes has clear implications for governmental flood defence policy, and makes the argument that flood defence schemes should not be planned and managed on a local scale, but instead a wider basin wide approach is needed.

As issues of energy security and environmental concerns gain public awareness, tidal energy extraction becomes a more viable option. However this thesis shows that the

amount of extractable energy that can be expected from a free stream tidal power plant may not remain constant, as the tidal response to SLR can be enough to change the current velocities.

Our simulations show that other coastal impacts such as land reclamation have had a significant impact on the basin wide coastal regime, furthermore this thesis has shown that changes to the coastline in the Bohai Sea may have made the basin more susceptible to the tidal impacts of SLR.

The maximum high water (and therefore the likely hood of an area flooding) is dependant on a combination of the mean water level, maximum tidal range and any pressure set-up caused by weather, most notably wind. Therefore, any changes in tidal range can affect the frequency and magnitude of a flood event.

6.1   Further Work and Recommendations

During this project a number of ideas have been developed, but due to time constraints it was not possible to take them any further. Here we discuss these ideas for future work.

Global simulations

It has been shown that secular trends in the tides can be simulated by the tidal models described in the thesis (Papers III and IV). However, previous studies have looked at the effect of SLR on the global tides (Green, 2010; Muller et al., 2011), but these results have failed to match observations (Muller et al., 2011) and we would suggest that the discrepancy is mainly due to resolution issues (Egbert et al., 2004; Green and Nycander, 2013).

The OTIS tidal model can be used for global simulations (for example see Egbert et al., 2004; Green, 2010) and increased computational power would allow high resolution ($1/30^o$ in latitude and longitude) simulations. Combining the most accurate bathymetry and GIA predictions should enable the best chance of reproducing secular tidal trends, as observed in the global tidal gauge database. This will also enable a sensitivity test of different bathymetric databases. If necessary/appropriate model tuning could be applied and future SLR runs could then be made.

Climatic feedbacks

It has been suggested that 50% of the mechanical input required to sustain the global over-turing circulation is provided by the tides through internal tides. Thus it is possible that any large-scale changes in the tidal regime and more specifically the tidal energy dissipation field may have climatic effects. This could use global high resolution tidal model runs and feed dissipation fields into a climate model such as OSUvic (Weaver et al., 2001) for the climate impact simulations.

The Taylor Problem as a validation technique

In order to asses how well our models work it is necessary to validate them. Generally this is done comparing them to observations (tide gauge or satellite altimetry). However, there are issues with this method. In some regions the coverage or/and data quality of tidal gauge data is poor, for example in seasonally ice covered regions only summer observations are possible. Satellite altimetry has improved data coverage but in regions that have undergone rapid tidal changes, the process of averaging over many years introduces inaccuracies (Paper III).

Tidal models, as most models, are highly dependant on the accuracy on the inputs i.e. bathymetric and boundary conditions. However, there are significant disagreements between bathymetric and elevation databases (see chapter 4.3). Therefore, there is a need for a more general form of tidal model validation that is independent of region and therefore bathymetery. Furthermore, while it is possible to test the model against observations in very realistic situations, it is more difficult to test the individual parametrisations or processes that are part of the model. For instance it is possible that two poor parametrisations are compensating for reach other and the results are therefore correct, but for the wrong reasons. The Taylor Problem as described by Taylor (1921) uses no bathymetry and simple boundary conditions, thus provides a input free a unique opportunity to compare the model solutions to analytical solutions in a highly idealized setting.

Is the relationship between SLR and changes in M_2 amplitude observable

While there has been many studies that have observed secular changes in the tidal

regime, and modeling studies that have linked this to SLR, there has not been a purely observational study that has linked SLR to changes in tidal regime. This partly due to the small size of the signal and the length of tidal gauge data required to get a significant response. However the UK has some of the longest tidal gauge records and results from Paper IV give us confidence that a direct relationship should be observable. Furthermore, the use of a GIA model will enable the response (and relationship to tidal changes) of retaliative SLR and eustatic SLR to be compared.

References

Accad, Y., Perekis, C., 1978. Solution of the tidal equations for the m2 and s2 tides in the world oceans from a knowledge of the tidal potential alone. Philosophical Transactions of the Royal Society of London. Series A, Mathematical and Physical Sciences 290, 235–266.

Arbic, B., Garner, S., Hallberg, R., Simmons, H., 2004. The accuracy of surface elevations in forward global barotropic and baroclinic tide models. Deep-Sea Research II 51, 3069–3101.

Arbic, B., Garrett, C., 2010. A coupled oscillator model of shelf and ocean tides. Continental Shelf Research 30, 564–574.

Arbic, B., Karsten, R., C.Garrett, 2009. On tidal resonance in the global ocean and the back-effect of coastal tides upon open-ocean tides. Atmosphere-Ocean 47 (4), 239–266.

Baines, P. G., 1982. On internal tide generation models. Deep-Sea Research 29, 307–338.

Baker, A., 1991. Tidal Power. Peter Peregrinus, London.

Bell, C., Vassie, J. M., Woodworth, P. L., 1999. POL/PSMSL tidal analysis software kit 2000 (TASK-2000). Tech. rep., Permanent Service for Mean Sea Level, Proudman Oceanographic Lab., Bidston Observatory, Birkenhead, Merseyside CH43 7RA, UK.

Blanchfield, J., Garrett, C., Rowe, A., Wild, P., 2008. Tidal stream power resource assessment for Masset Sound, Haida Gwaii. Proceedings of the Institution of Mechanical Engineers, Part A: Journal of Power and Energy 222 (5), 485–492.

Brown, T., 1987. Kelvin wave reflection at an oscillating boundary with applications to the North Sea. Continental Shelf Research 7 (4), 351–365.

Brown, T., 1989. On the general problem of Kelvin wave reflection at an oscillating boundary. Continental Shelf Research 9 (10), 931–937.

Bryden, I., Couch, S., 2006. Me1-marine energy extraction:tidal resource analysis. Renewable Energy 31, 133–139.

Bryden, I., Grinsted, T., Melville, G., 2004. Assessing the potential of a simple tidal channel to deliver useful energy. Applied Ocean Research 26, 198–204.

Cazenave, A., Llovel, W., 2010. Contemporary sea level rise. Annual reviews in marine science 2, 145–173.

Church, J., White, N., 2006. A 20th century acceleration in global sea-level rise. Geophysical Research Letters 33, L01602.

Church, J., White, N., 2011. Sea-level rise from the late 19th to the early 21st century. Surveys in Geophysics.

Creel, L., 2003. Ripple effects: popluation and coastal regions. Tech. rep., Population refrence bureau.

Darwin, G. H., 1899. The tides and kindred phenomena in the solar system. Houghton, Boston.

Denman, K., Brasseur, G., Chidthaisong, A., Ciais, P., Cox, P., Dickinson, R., Hauglustaine, D., Heinze, C., Holland, E., Jacob, D., Lohmann, U., Ramachandran, S., da Silva Dias, P., Wofsy, S., Zhang, X., 2007. In: Climate Change 2007: The Physical Science Basis. Contribution of Working Group I to the Fourth Assessment Report of the Intergovernmental Panel on Climate Change [S.Solomon and D. Qin and M. Manning and Z. Chen and M. Marquis and K.B. Averyt and M.Tignor and H.L. Miller (eds.)]. Cambridge University Press, Cambridge, United Kingdom and New York, NY, USA., Ch. Couplings Between Changes in the Climate System and Biogeochemistry.

Dickey, J., 1994. Lunar laser ranging: a continuing legacy of the Apollo program. Science 265, 482–490.

Dyke, P., 2001. Coastal and shelf sea modelling. Kluwer Academic Publishers.

Egbert, G., Bennett, A., Foreman, M., 1994. TOPEX/POSEIDON tides estimated using a global inverse model. Journal of Geophysical Research 99 (C12), 24821–24852.

Egbert, G., Erofeeva, S., 2002. Efficient inverse modeling of barotropic ocean tides. Journal of Atmospheric and Oceanic Technology 19 (2), 183–204.

Egbert, G., Ray, R., 2001. Estimates of m2 tidal energy dissipation from TOPEX/POSEIDON altimetry. Geophysical Research Letters 30 (10), 1907.

Egbert, G. D., Bills, B. G., Ray, R. D., 2004. Numerical modeling of the global semidiurnal tide in the present day and in the last glacial maximum. Journal of Geophysical Research 109, C03003, doi: 10.1029/2003JC001973.

Egbert, G. D., Ray, R. D., 2000. Significant tidal dissipation in the deep ocean inferred from satellite altimeter data. Nature 405, 775–778.

Egbert, G. D., Ray, R. D., 2003. Semidiurnal and diurnal tidal dissipation from TOPEX/POSEIDON altimetry. Geophysical Research Letters 3017, 1907, doi: 10.1029/2003GL017676.

Emery, W., Thomson, R., 2001. Data analysis methods in physical oceanography. Elsiver.

Flick, R., Murray, J., Ewing, L., 2003. Trends in United States tidal datum statistics and tide range. J. Waterw. Port Coastal Ocean Eng. 129, 155–164.

Fong, S., Heaps, N., 1978. Note on quater-wave resonance in the Bristol Channel. Institute of Oceanographic Science report 63.

Garret, C., 1972. Tidal resonance in the Bay of Fundy and Gulf of Maine. Nature 238, 441–443.

Garrett, C., 1972. Tidal resonance in the Bay of Fundy, Gulf of Maine. Nature 238, 441–443.

Garrett, C., 2003. Internal tides and ocean mixing. Science 301, 1858–1859.

Garrett, C., Cummins, P., 2005. The power potential of tidal currents in channels. Proceedings of The Royal Society 461, 2563–2572.

Garrett, C., Greenberg, D., 1977. Predicting changes in tidal regime: The open boundary problem. Journal of Physical Oceanography 7 (2), 171–181.

Glaser, R., Haberzettl, P., Walsh, R., 1991. Land reclamation in Singapore, Hong Kong and Macau. GeoJournal 24 (4), 365–373.

Godin, G., 1988. The resonance period of the Bay of Fundy. Continental Shelf Research 8, 1005–1010.

Godin, G., 1993. On tidal resonance. Continental Shelf Research 13, 89–107.

Govarets, A., Lauwerts, B., 2009. Assessment of the impact of coastal defence structures. Tech. rep., OSPAR commision.

Green, J., 2010. Ocean tides and resonance. Ocean Dynamics 60, 1243–1253.

Green, J., Huber, M., 2013a. Deep-time tidal mixing and its implication for the evolution of the Earth-Moon system. Submitted to EPSL.

Green, J., Huber, M., 2013b. Tidal dissipation in the early Eocene and implications for ocean mixing. in press for Geophysical Research Letters.

Green, J., Nycander, J., 2013. A comparison of tidal conversion parameterizations for tidal models. Journal of Physical Oceanography 43, 104–119.

Green, J. A. M., David, T. W., 2013. Modelling the tides in the South China sea without assimilation. Deep-Sea Research 78, 42–48.

Greenberg, D., 1979. A numerical model investigation of tidal phenomena in the Bay of Fundy and Gulf of Maine. Maine Geodsey 2, 161–187.

Greenberg, D., Blanchard, W., Smith, B., Barrow, E., 2012. Climate change, mean sea level and high tides in the Bay of Fundy. Atmpospheric-Ocean 50, 261–276.

Grinsted, A., Moore, J., Jevrejeva, S., 2009. Reconstructing sea level from paleo and projected temperatures 200 to 2100 ad. Climate Dynamics 34, 461–472.

Gustafsson, K. E., 2001. Computations of the energy flux to mixing processes via baroclinic wave drag on barotropic tides. Deep-Sea Research 48, 2283–2295.

Hasegawa, D., Sheng, J., Greenburg, D., Thompson, K., 2011. Far-field effects of tidal energy extraction in the Minas Passage on tidal circulation in the Bay of Fundy and Gulf of Maine using a nested-grid costal circulation model. Ocean Dynamics 61, 1845–1868.

Hendershott, M., 1972. The effects of solid earth deformation on global ocean tides. Geophys. J. R. Astron. Soc. 29, 389–402.

Hendershott, M., Speranza, A., 1971. Co-oscillating tides in long, narrow bays; the Taylor problem revisited. Deep-Sea Research 18, 959–980.

Hoeksema, R., 2007. Three stages in the history of land reclamation in the Netherlands. Irrigation and Drainage 56, S113–S126.

Holgate, S., 2007. On the decadal rates of sea level change during the twentieth century. Geophysical Research Letters 34, L01602.

Hollebrandse, F., 2005. Temporal development of the tidal range in the southern North Sea. Master's thesis, Delft University of Technology.

Holt, J., Wakelin, S., Lowe, J., J. Tinker, . .-. .-., 2010. The potential impacts of climate change on the hydrography of the northwest European continental shelf. Progress in Oceanography 86 (3–4), 361–379.

Jay, D., 2009. Evolution of tidal amplitudes in the eastern Pacific Ocean. Geophysical Research Letters 36, L04603.

Jayne, S., l.C. Laurent, 2001. Parameterizing tidal dissipation over rough topography. Geophysical Research Letters 28, 811–814.

Jeffreys, H., 1920. Tidal friction in shallow seas. Philosophical Transactions of the Royal Society of London: A 221, 239.

Kantha, L., Clayson, C., 2000. Numerical Models of Oceans and Oceanic Processes. Academic Press.

Karsten, R., McMillan, J., Lickley, M., Haynes, R., 2008. Assesment of tidal current energy in the Minas Passage, Bay of Fundy. Proccedings of the IMechE, Part A: Journal of Power and Energy 222, 493–507.

Kirby, R., Retiï¿½$\frac{1}{2}$re, C., 2009. Comparing environmental effects of Rance and Severn barrages. Proceedings of the ICE - Maritime Engineering 162 (1), 11–26.

Kopp, R., Simons, F., Mitrovica, J., Maloof, A., Oppenheimer, M., 2009. Probabilistic assessment of sea level during the last interglacial stage. Nature 462, 863–867.

Ku, L., Greenberg, D., Garret, C., Dobson, F., 1985. Nodal modulation of the lunar semidiurnal tide in the Bay of Fundy and Gulf of Maine. Science 230, 69–71.

Kunze, E., Rosenfeld, L. K., Carter, G. S., Gregg, M. C., 2002. Internal waves in monterey submarine canyon. Journal of Physical Oceanography 32, 1890–1913.

Kvale, E., 2006. The origin of neap-spring tidal cycles. Marine Geology 235 (1–4), 5–18.

Laurent, L. C. S., Garrett, C., 2002. The role of internal tides in mixing the deep ocean. Journal of Physical Oceanography 24, 1105–1117.

LeProvost, C., Genco, M., Lyard, F., Vincent, P., Canceil, P., 1994. Spectroscopy of the world ocean tides from a finite element hydrodynamic model. Journal of Geophysical Research 99, 24777–24797.

Leuliette, E., Nerem, R., Mitchum, G., 2004. Calibration of TOPEX/Poseidon and Jason altimeter data to construct a continuous record of mean sea level change. Marine Geodesy 27 (1-2), 79–94.

Li, X., Sun, X., Wang, S., Ye, F., Li, Y., Li, X., 2011. Characteristic analysis of Tianjin offshore tide. Marine Science Bulletin (english edition) 13 (40–49).

Lyard, F., Genco, M., 1994. Optimization methords for bathymetry and open bounday conditions in a finite element model of ocean tides. Journal of Computor Physics 114, 234–256.

Miller, G., 1966. The flux of tidal energy out of the deep ocean. Journal of Geophysical Research 71, 2485–2489.

Miller, R., 2007. Numerical modeling of ocean circulation. Cambridge Univeristy Press.

Muller, M., Arbic, B., Mitrovica, J., 2011. Secular trends in ocean tides: Observations and model results. Journal of Geophysical Research 116, C05013.

Munk, W., 1997. Once again: Once again - tidal friction. Progress in Oceanography 40 (1-4), 7–35.

Munk, W., MacDonald, G., 1960. The rotation of the Earth a Geophysical Dissusion. Cambridge University Press.

Munk, W., Wunch, C., 1998. Abyssal recipes II: energetics of tidal and wind mixing. Deep-Sea Research 45, 1977–2010.

Nash, J. D., Alford, M. H., Kunze, E., 2005. On estimating internal-wave energy fluxes in the ocean. Journal of atmospheric and oceanic technology 22, 1551–1570.

Neill, S., Litt, E., Couch, S., Davies, A., 2009. The impact of tidal stream turbines on large-scale sediment dynamics. Renewable Energy 34 (12), 2803–2812.

Ni, J., Borthwick, A., Qin, H., 2002. Intergrated approach to determining postreclamation coastlines. Journal of Enviromental Engineering 128 (6), 543–551.

Nicholls, R., Hanson, S., Lowe, J., Warrick, R., Lu, X., Long, A., Carter, T., 2011a. Constructing sea-level scenarios for impact and adaptation assessment of coastal area: A guidance document. supporting material. Tech. rep., Intergovernmental Panel on Climate Change Task Group on Data and Scenario Support for Impact and Climate Analysis (TGICA).

Nicholls, R., Marinova, N., Lowe, J., Brown, S., Vellinga, P., Gusmï¿½$\frac{1}{2}$o, D., Hinkel, J., Tol, R., 2011b. Sea-level rise and its possible impacts given a 'beyond $4^o c$ world' in the twenty-first century. Phil. Trans. R. Soc. A 369 (1934), 161–181.

Nycander, J., 2005. Generation of internal waves in the deep ocean by tides. Journal of Geophysical Research 110, C10028, doi:10.1029/2004JC002487.

Oley, L. Y., 2005. A wetting and drying scheme for POM. Ocean Modelling 9, 133–150.

Pethick, J., Morris, R., Evans, D., 2009. Nature conservation implications of a Severn tidal barrage - a preliminary assessment of geomorphological change. Journal for Nature Conservation 17, 183–198.

Pfeffer, W., Harper, J., O'Neel, S., 2008. Kinematic constraints on glacier contributions to 21st-century sea-level rise. Science 321, 1340–1343.

Pickering, M., Wells, N., Horsburgh, K., 2012. The impact of future sea-level rise on the European Shelf tides. Continental Shelf Research, doi:10.1016/j.csr.2001.11.011.

Pickles, A., Tosen, R., 1998. Settlement of reclaimed land for the new Hong Kong international airport. Geotechnical Engineering, Proceedings of the Institution of Civil Engineers 4, 191–209.

Provst, C. L., 1991. Generation of over-tides and compound tides (review). Tidal hydro-dynamics, 269–295.

Pugh, D., 1981. Tidal amphidrome movement and energy dissipation in the Irish Sea. Geophysical Journal International 67 (2), 515–527.

Pugh, D. T., 1996. Tides, surges and mean sea level. Wiley.

Rahmstorf, S., 2007. A semi-empirical approach to projecting future sea-level rise. Science 315, 368–370, 10.1126/science.1135456.

Ray, R., 1998. Ocean self-attraction and loading in numerical tidal models. Marine Geodesy 21 (3), 181–192.

Ray, R., 2009. Secular changes in the solar semidiurnal tide of the western North Atlantic Ocean. Geophysical Research Letters 36, L19601.

Ray, R., Eanes, R., Chao, B., 1996. Detection of tidal dissipation in the solid earth satallite tracking and alitmetery. Nature 381 (595–597).

Retiere, C., 1994. Tidal power and the aquatic enviroment of La Rance. Biological Journal of the Linnean Society 51, 25–36.

Rienecker, M., Teubner, M., 1980. A note on frictional effects in Taylor's problems. Journal of Marine Research 38, 183–191.

Rizal, S., 2002. Taylor's problem – influences in the spatial distribution of real and virtual amphidromes. Continental Shelf Research 22, 2147–2158.

Rohling, E., Grant, K., Hemleben, C., Siddall, M., Hoogakker, B., Bolshaw, M., Kucera, M., 2008. High rates of sea-level rise during the last interglacial period. Nature Geoscience 1, 38–42.

Roos, P., Velema, P. C. R., Hulscher, S. J. M. H., Stolk, A., 2011. An idealized model of tidal dynamics in the North Sea: resonance properties and response to large-scale changes. Ocean Dynamics 61, 2019–2035.

Schouten, J., 2006. Technical feasibility of a large-scale land reclamation. Master's thesis, Delft University of Technology.

Schwiderski, E., 1978. Global ocean tides. part i. a detailed hydrodynamical interpolation model. NAVAL SURFACE WEAPONS CENTER DAHLGREN LAB VA.

SDC, 2007. Turning the tide: Tidal power in the uk. Tech. rep., Sustainable Development Commission.

Sjï¿½½berg, B., Stigebrandt, A., 1992. Computations of the geographical distribution of the energy flux to mixing processes via internal tides: its horizontal distribution and the associated vertical circulation in the ocean. Deep-Sea Research 39, 269–291.

Smith, W., Sandwell, D., 1997. Global seafloor topographyfrom satellite altimetry and ship depth soundings. Science 277, 1956–1962.

So, C., 1986. Reclamation and its impact on current flows in Hong Kong. Dock Harbour Authority 67 (784), 149–155.

Stepanov, V., Hughes, C. W., 2004. Parameterization of ocean self-attraction and loading in numerical models of the ocean circulation. Journal of Geophysical Research 109, C03037.

Stewart, R. H., 2007. Introduction To Physical Oceanography. Texas A&M University. 345pp. Available from `http://oceanworld.tamu.edu/ocean410/ocng410_text_book.html`.

Sutherland, G., Foreman, M., Garrett, C., 2007. Tidal current energy assessment for Johnstone Strait, Vancouver Island. Poc.IMechE 221 (Part A: J.Power and Energy), 147–157.

Taylor, G., 1919. Tidal friction in the Irish Sea. Philosophical Transactions of the Royal Society of London: A 220, 1–93.

Taylor, G., 1921. Tidal oscillations in gulfs and rectangular basins. Proceedings of the London mathmatical Society 20 (2), 148–181.

Uehara, K., Saito, Y., 2003. Late quaternary evolution of the Yellow/East China sea tidal regime and its impacts on sediments dispersal and seafloor morphology. Sediment Geology 162, 25–38.

Uehara, K., Scourse, J. D., Horsburgh, K. J., Lambeck, K., Purcell, A. P., 2006. Tidal evolution of the northwest European shelf seas from the Last Glacial Maximum to the present. Journal of Geophysical Research 111, C09025, doi: 10.1029/2006JC003531.

UNEP, 2006. Marine and coastal ecosystems and human wellbeing: A synthesis report based on the findings of the millennium ecosystem assessment. Tech. rep., UNEP.

Vemeer, M., Rahmstof, S., 2009. Global sea levels linked to global temperatures. Proc. Natl. Acad. Sci. USA 106, 21527–21532.

Walkington, I., Burrows, R., 2009. Modelling tidal stream power potential. Applied Ocean Research, 31 (4), 239–245.

Ward, R., 2010. General bathymetric charts of the ocean. Hydro-International 14 (5).

Ward, S., Green, J., Pelling, H., 2012. Shelf sea dynamics and tidal power plants on the European Shelf with future sea level rise. Ocean Dynamics, DOI 10.1007/s10236–012–0552–6.

Weaver, A., Eby, M., Wiebe, E., Bitz, C., Duffy, P., Holland, T. E. A. F. M., MacFadyen, A., Saenko, O., Schmittner, A., Wang, H., Yoshimori, M., 2001. The UVic earth system climate model: Model description, climatology and applications to past, present and future climates. Atmos.-Ocean 4 (361–428).

Wolf, J., Walkington, I. A., Holt, J., Burrows, R., 2009. Enviromental impacts of tidal power schemes. Proceedings of the ICE - Maritime Engineering 162 (4), 165–177.

Woodworth, P., Gehrels, W., Nerem, R., 2011. Nineteenth and twentieth century changes in sea level. Oceanography 24, 80–93.

Woodworth, P., Teferle, N., Bingley, N., Sherman, R., Williams, S., 2009. Trends in UK tidal guages revisited. Geophysical Journal International 179, 19–30.

Wright, J., Colling, A., Park, D., 1999. Waves, tides and shallow water processes. Open University.

Young, E., Aldridge, J., Brown, J., 2000. Development and validation of a three-dimensional curvilinear model for the study of fluxes through the North Channel of the Irish Sea. Continental Shelf Research 20, 997–1035.

Zaron, E., Egbert, G., 2006. Estimating open-ocean barotropic tidal dissipation: The Hawaiian Ridge. Journal of Physical Oceanography 36, 1019–1035.

Zhang, J., Wang, J., 1999. Combined impacts of msl rise and the enlarged tidal range on the engineering design standard in the areas around the Huanghe River mouth. Marine Science Bulletin 18 (5), 1–9.

Part III

Papers I-IV

"I must go down to the seas again, for the call of the running tide
Is a wild call and a clear call that may not be denied;
And all I ask is a windy day with the white clouds flying,
And the flung spray and the blown spume, and the sea-gulls crying."

- Sea Fever, J. Masefield

Paper I

Paper II

Paper III

Paper IV